AMERICAN SOCIETY FOR MICROBIOLOGY | Antimicrobial Agents and Chemotherapy®

ANTIVIRAL AGENTS

Overcoming Culture Restriction for SARS-CoV-2 in Human Cells Facilitates the Screening of Compounds Inhibiting Viral Replication

Santseharay Ramirez,[a,b] Carlota Fernandez-Antunez,[a,b] Andrea Galli,[a,b] Alexander Underwood,[a,b] Long V. Pham,[a,b] Line A. Ryberg,[a,b] Shan Feng,[a,b] Martin S. Pedersen,[a,b,c] Lotte S. Mikkelsen,[a,b] Sandrine Belouzard,[d,e] Jean Dubuisson,[d,e] Christina Sølund,[a,b,f] Nina Weis,[f,g] Judith M. Gottwein,[a,b] Ulrik Fahnøe,[a,b] Jens Bukh[a,b]

[a]Copenhagen Hepatitis C Program (CO-HEP), Department of Infectious Diseases, Copenhagen University Hospital, Hvidovre, Copenhagen, Denmark
[b]Copenhagen Hepatitis C Program (CO-HEP), Department of Immunology and Microbiology, Faculty of Health and Medical Sciences, University of Copenhagen, Copenhagen, Denmark
[c]Department of Clinical Microbiology, Copenhagen University Hospital, Hvidovre, Copenhagen, Denmark
[d]University of Lille, CNRS, Inserm, CHU Lille, Lille, France
[e]Centre d'Infection et d'Immunité de Lille, Institut Pasteur de Lille, Lille, France
[f]Department of Infectious Diseases, Copenhagen University Hospital, Hvidovre, Copenhagen, Denmark
[g]Department of Clinical Medicine, Faculty of Health and Medical Sciences, University of Copenhagen, Copenhagen, Denmark

ABSTRACT Efforts to mitigate the coronavirus disease 2019 (COVID-19) pandemic include the screening of existing antiviral molecules that could be repurposed to treat severe acute respiratory syndrome coronavirus 2 (SARS-CoV-2) infections. Although SARS-CoV-2 replicates and propagates efficiently in African green monkey kidney (Vero) cells, antivirals such as nucleos(t)ide analogs (NUCs) often show decreased activity in these cells due to inefficient metabolization. SARS-CoV-2 exhibits low viability in human cells in culture. Here, serial passages of a SARS-CoV-2 isolate (original-SARS2) in the human hepatoma cell clone Huh7.5 led to the selection of a variant (adapted-SARS2) with significantly improved infectivity in human liver (Huh7 and Huh7.5) and lung cancer (unmodified Calu-1 and A549) cells. The adapted virus exhibited mutations in the spike protein, including a 9-amino-acid deletion and 3 amino acid changes (E484D, P812R, and Q954H). E484D also emerged in Vero E6-cultured viruses that became viable in A549 cells. Original and adapted viruses were susceptible to scavenger receptor class B type 1 (SR-B1) receptor blocking, and adapted-SARS2 exhibited significantly less dependence on ACE2. Both variants were similarly neutralized by COVID-19 convalescent-phase plasma, but adapted-SARS2 exhibited increased susceptibility to exogenous type I interferon. Remdesivir inhibited original- and adapted-SARS2 similarly, demonstrating the utility of the system for the screening of NUCs. Among the tested NUCs, only remdesivir, molnupiravir, and, to a limited extent, galidesivir showed antiviral effects across human cell lines, whereas sofosbuvir, ribavirin, and favipiravir had no apparent activity. Analogously to the emergence of spike mutations *in vivo*, the spike protein is under intense adaptive selection pressure in cell culture. Our results indicate that the emergence of spike mutations will most likely not affect the activity of remdesivir.

KEYWORDS A549 cells, COVID-19, coronavirus, galidesivir, Huh7.5 cells, molnupiravir, nucleotide analogs, remdesivir, sofosbuvir, virus evolution

Severe acute respiratory syndrome coronavirus 2 (SARS-CoV-2), responsible for the coronavirus disease 2019 (COVID-19) outbreak, was first identified in China in early 2020 (1) but rapidly spread to the rest of the world, causing a pandemic that has resulted in millions of deaths (2). Although a hallmark of COVID-19 is the development

Citation Ramirez S, Fernandez-Antunez C, Galli A, Underwood A, Pham LV, Ryberg LA, Feng S, Pedersen MS, Mikkelsen LS, Belouzard S, Dubuisson J, Sølund C, Weis N, Gottwein JM, Fahnøe U, Bukh J. 2021. Overcoming culture restriction for SARS-CoV-2 in human cells facilitates the screening of compounds inhibiting viral replication. Antimicrob Agents Chemother 65:e00097-21. https://doi.org/10.1128/AAC.00097-21.

Address correspondence to Santseharay Ramirez, santseharayra@sund.ku.dk, or Jens Bukh, jbukh@sund.ku.dk.

Received 21 January 2021
Returned for modification 17 February 2021
Accepted 20 April 2021
Accepted manuscript posted online 26 April 2021
Published 17 June 2021

of respiratory symptoms from mild upper airway affection to life-threatening pneumonia, additional distinctive features of the disease are vascular changes (3) and numerous extrapulmonary manifestations and systemic complications (4). SARS-CoV-2 might indeed be able to infect different organs, as the virus genetic material has been detected in various tissues (5).

SARS-CoV-2 has been classified within the *Coronaviridae* family, the *Betacoronavirus* genus, and the *Sarbecovirus* subgenus (6). It is most closely related to SARS-like betacoronaviruses of bat origin, but its genomic organization is very similar to that of the well-characterized SARS-CoV (1). Its genome consists of a long positive-sense, single-strand RNA molecule of approximately 30 kb, following the classical genomic organization of viruses belonging to this family, with untranslated regions (UTRs) at the 5′ and 3′ ends and numerous open reading frames (ORFs) throughout the coding sequences (1). Separate ORFs encode the structural virion components, including the spike glycoprotein (S), the envelope (E), the membrane (M), and the nucleocapsid (N), as well as various accessory proteins (1). The largest ORFs (ORF1a and -1ab) encode the nonstructural proteins (nsp's) of the virus, responsible for the RNA synthesis machinery (1). The viral RNA-dependent RNA polymerase (nsp12) is an attractive drug target for antiviral therapy. However, identifying nucleos(t)ide analogs (NUCs) with anticoronavirus activity is challenged by the 3′-to-5′ proofreading exoribonuclease activity of the nsp14 protein, and only a very limited number of molecules have been shown to overcome this unique feature (7).

Drug repurposing, compared to *de novo* drug discovery, significantly shortens the time and reduces the cost of developing antivirals for emerging pandemic viral diseases. Two of the antiviral molecules that inhibit SARS-CoV-2 and other pandemic coronaviruses are the broad-spectrum antivirals remdesivir and β-D-N^4-hydroxycytidine (NHC) (molnupiravir), which were initially part of antiviral discovery programs for the treatment of hepatitis C virus (HCV) infection (8, 9). Remdesivir is now included in the standard-of-care treatment of COVID-19 patients in several countries. It is therefore relevant to continue searching for such compounds, focusing on the molecules that exhibit a good safety profile in humans and developing appropriate models for their preclinical screening in cell culture.

Although SARS-CoV-2 has been found in epithelial cells in the upper respiratory tract and in the lungs and other tissues in infected individuals, established human cell culture lines poorly support SARS-CoV-2 production (10). Various clones of the African green monkey kidney cell line "Vero" support high levels of SARS-CoV-2 replication and propagation; however, not being a human cell line, Vero cells show limitations for drug screening, especially for the screening of prodrugs that have been designed to be metabolized in human cells (11). Calu-3, a non-small-cell lung cancer cell line (12), supports SARS-CoV-2 infection and replication with viral particle production but at significantly lower levels than those observed in Vero cells (11, 13). Overexpression of human ACE2 (hACE2) in the lung adenocarcinoma cell line A549 permits infection with SARS-CoV-2 (14, 15). Additionally, CaCo-2, a colorectal adenocarcinoma cell line, has been shown to support the replication and production of infectious SARS-CoV-2 particles (16).

Other viruses, such as HCV, also exhibit restricted culture viability, and efficient replication and propagation of adapted viruses are limited to specific clones derived from human hepatoma cell lines (Huh7), including the Huh7.5 cell line (17, 18).

In this study, we aimed to establish more efficient and robust platforms for the culture of SARS-CoV-2 in human cells through viral adaptation to overcome nonnatural culture restrictions, as an alternative to modifying the cells by overexpressing host factors. Overcoming the barrier for efficient culture of SARS-CoV-2 in human cells could benefit basic investigations in this research field and facilitate the preclinical screening of antiviral compounds.

RESULTS

Characterization of a COVID-19-associated SARS-CoV-2 isolate (SARS-CoV-2/human/Denmark/DK-AHH1/2020) in Vero E6 cells. Vero E6 cells, which permit the isolation of SARS-CoV-2 with high efficiency, were used to obtain the initial virus stock.

Cells were inoculated with a diluted nasopharyngeal sample from a COVID-19 patient diagnosed with SARS-CoV-2 infection. On day 3 after inoculation, cell cytopathic effect (CPE) was observed, which peaked at day 7. At first, CPE was characterized by the presence of syncytia, followed by the appearance of moderate cell death. Severe CPE with significant cell death was not observed until days 6 to 7. Culture supernatants were harvested daily during the first 5 days of the experiment, and the infectivity titers (expressed as $\log_{10}$ 50% tissue culture infectious doses [$TCID_{50}$] per milliliter) peaked at day 4 at 6.4 $\log_{10}$ $TCID_{50}$/ml.

A second-passage (passage 2 [P2]) virus stock (generated as described in Materials and Methods), which is referred to as $P2^{VeroE6}$ or original-SARS2, was further characterized and used for the additional experiments described below. The infectivity titer of the $P2^{VeroE6}$ virus stock was 5.5 $\log_{10}$ $TCID_{50}$/ml.

We determined the near-complete SARS-CoV-2 genome sequences, including the entire 5′ UTR (the 3′ UTR lacked the last nucleotide and the polyA sequence), of the original virus from the clinical sample (swab) and the $P2^{VeroE6}$ virus. As shown in Table 1, the isolate SARS-CoV-2/human/Denmark/DK-AHH1/2020 (GenBank accession no. MZ049597), referred to here as SARS-CoV-2_DK-AHH1 or DK-AHH1, exhibits only 10 nucleotide (nt) differences compared to the reference sequence of the Wuhan-Hu-1 isolate (GenBank accession number NC_045512.2). Among these, 6 differences lead to amino acid changes in the nsp2, nsp12, S, ORF3a, and N genomic regions. SARS-CoV-2_DK-AHH1 harbors the high-frequency polymorphisms D614G in S, which is now dominant throughout the world and has been linked to increased infectivity in cell culture and in animal models (19, 20), and P323L in nsp12, which has not yet been clearly linked to any phenotype. Compared to the original swab sample, the $P2^{VeroE6}$ virus was remarkably similar, with only four evolving nucleotide positions (Table 1). However, further serial passage of the virus in Vero E6 cells (P7) led to the emergence of several mutations throughout the genome, including an insertion of 3 amino acids in the S protein (Table 1). Moreover, the original Vero E6 culture inoculated with the COVID-19 swab sample was maintained for over a month, showing persistent infection with SARS-CoV-2 (Fig. 1A). Analysis of the viral sequence in the supernatants harvested at day 42 postinoculation revealed several new mutations, including 7 substitutions in the S protein (Table 1). Of those, E484D was present in over 95% of the viral population. Thus, we concluded that SARS-CoV-2 mutates during culture in Vero E6 cells, during serial passage, as well as during persistent infection.

SARS-CoV-2 can be adapted to efficient growth in human hepatoma cells (cell clone Huh7.5). We performed inoculations of Huh7.5 cells with the original $P2^{VeroE6}$ virus to determine the susceptibility and permissiveness of this human cell line, which has been proven to be key for the cell culture adaptation of HCV (18). The virus was serially passaged 6 times (Fig. 1A). We observed that the emergence of CPE occurred earlier and was more evident as the passage number increased, suggesting viral adaptation. In passage 1, CPE was not observed until day 8 postinfection, and the magnitude of the CPE was low at this time, with only minor changes in the morphology of the cells. In contrast, the CPE observed in the passage 6 culture was significantly higher, with massive cell death by day 4 postinfection. A viral stock was prepared from the 5th passage and further characterized (this virus is referred to as $P5^{Huh7.5}$ or adapted-SARS2 here).

We next performed a comparative titration of the original $P2^{VeroE6}$ and the adapted $P5^{Huh7.5}$ viruses in various cells (Fig. 1B). Increases of more than 3 logs (means of 4.7 and 8.0 $\log_{10}$ $TCID_{50}$/ml, respectively) in infectivity titers after adaptation were observed in Huh7.5 cells. Adapted-SARS2 also exhibited significantly increased titers in Vero E6 cells (mean of 7.0 $\log_{10}$ $TCID_{50}$/ml for adapted-SARS2 versus 5.5 $\log_{10}$ $TCID_{50}$/ml for original-SARS2). Interestingly, original-SARS2 was less viable in the Huh7 parental cell line than in the Huh7.5 clone; however, adaptation to the Huh7.5 clone also led to significant increases in infectivity titers in Huh7 cells (3.8 and 7.7 $\log_{10}$ $TCID_{50}$/ml for the original and adapted viruses, respectively).

Visual observations of cultures infected with adapted-SARS2 versus original-SARS2 (light microscope) suggested an increase in CPE. To better quantify this, we performed viral CPE assays (Fig. 1C) in which we detected for adapted-SARS2 an evident increase

TABLE 1 Sequence comparison between the Wuhan-Hu-1 and recovered DK-AHH1 viruses in Vero E6 cells[a]

Nucleotide position	Nucleotide(s) in Wuhan-Hu-1	Nucleotide change	Frequency in original swab sample (%)	Frequency in $P2^{VeroE6}$ virus (%)	Frequency in $P7^{VeroE6}$ virus (%)	Frequency in day 42^{VeroE6} virus (%)	Amino acid change	Genomic region
71	C	T	•	6.3	6.6	4.5	—	5′ UTR
241	C	T	99.7	99.6	99.3	99.4	—	5′ UTR
1059	C	T	99.9	99.7	99.5	99.9	T→I	nsp2
3037	C	T	99.6	99.4	99.3	99.6	—	nsp3
7348	T	G	•	•	•	11.3	N→K	nsp3
7480	C	T	•	•	•	5.8	—	nsp3
8025	C	T	•	•	11.1	•	A→V	nsp3
10465	G	A	99.8	99.7	99.5	99.8	—	nsp5
11001	C	T	•	•	•	21.7	T→I	nsp6
11504	G	A	•	•	•	84.8	V→I	nsp6
11522	T	G	•	•	15.6	•	F→V	nsp6
14408	C	T	99.8	99.7	99.6	99.8	P→L	nsp12
19170	C	T	•	3.8	99.6	•	—	nsp14
21646	C	T	0.6	9.9	•	•	—	S
21742	C	T	99.8	99.8	99.8	99.8	—	S
22203	G	GTAAACGGG	•	•	99.9	•	IN3	S
22206	A	G	•	•	•	7.7	D→G	S
22343	G	C	•	•	•	99.3	G→R	S
22487	G	A	81.8	56.9	•	90.5	E→K	S
23014	A	C	•	•	•	95.9	E→D	S
23403	A	G	99.9	99.7	99.6	99.7	D→G	S
23606	C	T	•	•	91.8	•	R→W	S
23615	C	A	•	•	7.6	•	R→S	S
23685	C	T	•	•	•	23.1	S→F	S
24138	C	T	•	•	•	5.2	T→I	S
24209	A	G	•	•	•	5.6	T→A	S
24538	A	C	•	•	•	99.8	Q→H	S
24632	C	T	•	•	•	5.2	L→F	S
25563	G	T	99.9	99.8	99.7	99.9	Q→H	ORF3a
26324	T	C	•	•	•	99.7	L→S	E
26333	C	T	•	•	5.2	•	T→I	E
26369	A	G	•	•	38.5	•	Y→C	E
26447	C	T	•	•	9.9	•	S→F	E
27229	A	G	•	•	10.5	•	T→A	ORF6
28899	G	T	99.9	99.5	99.3	99.2	R→I	N
29580	CTTTTCCGT	C	•	•	•	90.4	8-nt frameshift	ORF10

[a]Original swab refers to the sequence from the patient diagnosed with SARS-CoV-2. $P2^{VeroE6}$ and $P7^{VeroE6}$ refer to the stocks of the second passage and seventh passage on day 3 in Vero E6 cells. Day 42^{VeroE6} refers to the virus harvested from the inoculated Vero E6 culture at 42 days postinoculation. For the swab and $P2^{VeroE6}$, the complete SARS-CoV-2 genome (complete 5′UTR; 3′UTR missing the last nucleotide and the polyA sequence) was analyzed, whereas for the remaining samples, a nearly full-length sequence was obtained (missing the first 32 and the last 66 nucleotides including the polyA sequence). Differences (cutoff of 5%) are specified by the nucleotide position (number) according to the reference sequence of the Wuhan-Hu-1 isolate (GenBank accession number NC_045512.2), followed by the specific nucleotide in the reference sequence and in the DK-AHH1 isolate. The frequencies of changes in the sequences of the analyzed viruses (percentage of the reads) are shown in the next four columns. Sequence identity to the reference is represented by a dot. Nucleotide sequences were translated *in silico*, and if the nucleotide changes led to a substitution, the corresponding amino acid is indicated (original amino acid→new amino acid). Synonymous changes are represented with —. "IN3" indicates an insertion of 3 amino acids. The genomic region for each change is also indicated.

in CPE titers (log_{10} 50% cytopathic effect [CPE_{50}] per milliliter) in all cell lines. CPE significantly increased from 4.6 to 6.2 log_{10} CPE_{50}/ml in Vero E6 cells. In Huh7.5 cells, original-SARS2 was noncytopathic (we obtained a value just above the assay threshold in one of the independent experiments), whereas adapted-SARS2 led to high titers of 7.3 log_{10} CPE_{50}/ml. A similar effect was observed in the Huh7 parental cells (from undetectable to 6.1 log_{10} CPE_{50}/ml).

In addition to the increases in infectivity and CPE titers observed after infection with adapted-SARS2 in Huh7.5 cells, we also noticed evident increases in the intensity of antigen staining using anti-spike protein antibody (Ab) and in the number of infected cells at noncytopathic virus dilutions of adapted-SARS2 compared to original-SARS2 (Fig. 1D). Thus, adapted-SARS2 might both replicate and propagate at higher levels in Huh7.5 cells, as also indicated by the significant increase in CPE titers. In

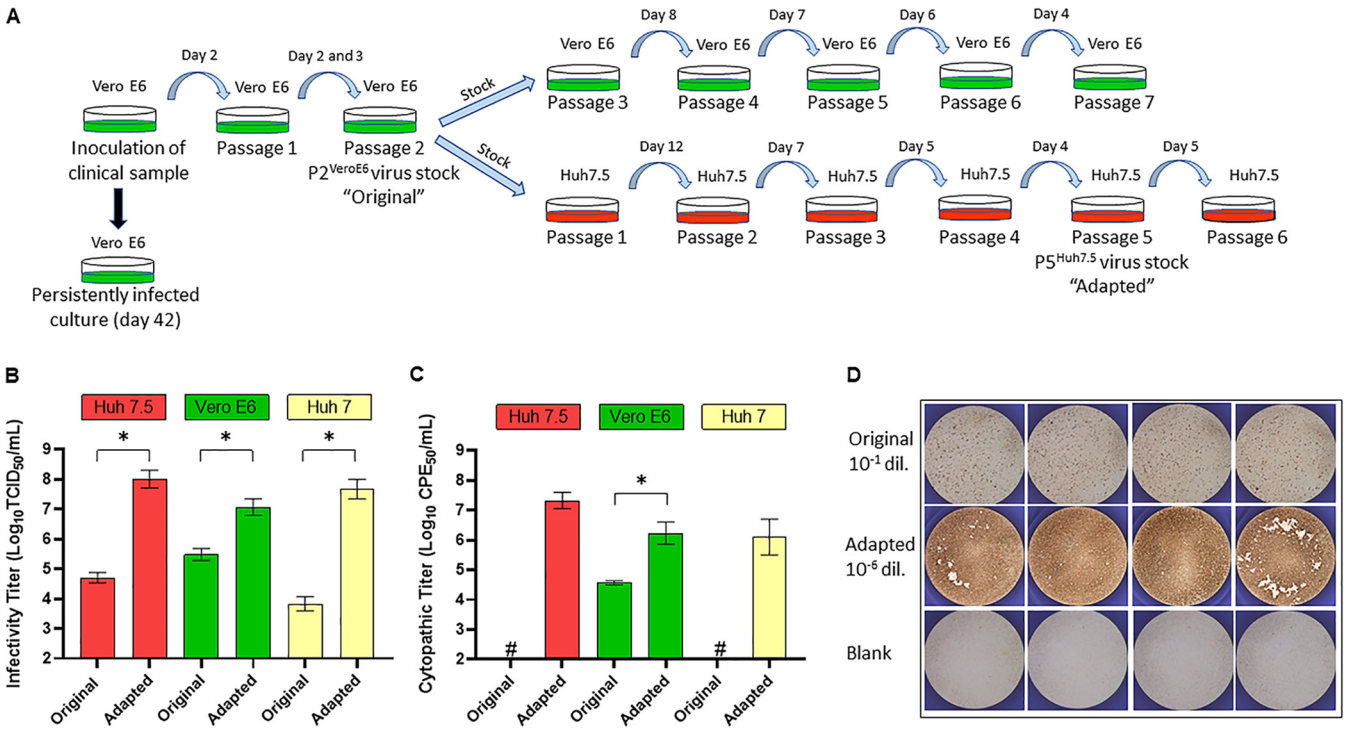

FIG 1 Adaptation of SARS-CoV-2 to efficient growth in Huh7.5 cells. (A) Schematic overview of the serial passages performed in Vero E6 and Huh7.5 cells. Dishes represent the culture surfaces, and green and red represent Vero E6 and Huh7.5 cells, respectively. The day of supernatant harvest used for passage is indicated above the light blue arrow that symbolizes the transfer of the culture supernatant to naive (uninfected) cells. The black arrow indicates "no passage." (B) Comparative infectivity titers of the $P2^{VeroE6}$ (original) and $P5^{Huh7.5}$ (adapted) viruses in Huh7.5, Vero E6, and Huh7 cells. Infectivity titers (log_{10} $TCID_{50}$ per milliliter) are shown on the *y* axis. Results are based on several independent experiments: for original and adapted viruses in Huh7.5 cells, 6 and 2 independent experiments with 4 replicates each are represented, respectively. In a third independent titration experiment, endpoint dilution for the adapted virus was not achieved (>7 log_{10} $TCID_{50}$/ml), and thus, the data were not included in the graph. For the Vero E6 cells, the data presented in the graph correspond to 5 (original) and 4 (adapted) independent experiments with 4 replicates each. For the parental Huh7 cells, results are based on 3 independent experiments for each virus. Bars represent the means and standard errors of the means (SEM) from the different independent experiments. Statistical significance ($P < 0.05$ by an unpaired *t* test) is highlighted with an asterisk. (C) Comparative cytopathic effect titers of the original and adapted viruses in Huh7.5, Vero E6, and Huh7 cells. Cytopathic effect titers (log_{10} CPE_{50} per milliliter) are shown on the *y* axis. For original and adapted viruses in both Huh7.5 and Vero E6 cells, results are based on 3 independent experiments with 4 replicates each. For the original virus in Huh7.5 cells, only one experiment yielded a CPE value over the threshold, and thus, the value was not plotted (depicted with "#"). In the case of the parental Huh7 cells, results are based on 3 independent experiments as well, and none of the experiments with the original virus yielded values over the assay threshold (#). Bars represent the SEM for the different independent experiments. Statistical significance ($P < 0.05$ by an unpaired *t* test) is highlighted with an asterisk. (D) Visual comparative SARS-CoV-2 antigen staining of both original and adapted viruses after infection of Huh7.5 cells or the blank (noninfected cells), from a representative $TCID_{50}$ assay. Each picture represents a replicate of infections performed at the indicated dilutions (noncytopathic) for each virus and was obtained after HRP staining with an anti-spike protein antibody, using the ImmunoSpot series 5 UV analyzer as described in Materials and Methods.

contrast, no such evident differences were observed upon infection of Vero E6 cells with adapted-SARS2 despite the increase in infectivity titers (data not shown).

The nearly complete genome sequence of the Huh7.5-adapted-SARS2 (P1, P5, and P6) was obtained and analyzed. We found mutations leading to amino acid changes in several genomic regions compared to original-SARS2 (Table 2). The region coding for the spike protein accumulated a significant number of high-frequency (>90% of the viral population) changes, including a deletion leading to the removal of 9 amino acids in the N-terminal domain (from nt 21762 to nt 21788) and 3 nonsynonymous mutations: A23014C (E484D amino acid change according to S-protein-specific numbering), C23997G (P812R), and A24424C (Q954H). The deletion and the E484D substitution were already dominant (frequency of >90%) after the first passage in Huh7.5 cells ($P1^{Huh7.5}$) (Table 2).

Outside S, the only other positions in which we found a clear indication of significant evolution at the amino acid level (that is, a sustained increase in the frequency of a residue over the three analyzed Huh7.5 passages) were T11522G (F184V in nsp6), C19895T (A92V in nsp15), C26333T (T30I in E), and C28331T (P20S in N) (Table 2). The

TABLE 2 Sequence analysis of SARS-CoV-2 harvested after passage in Huh7.5 cells[a]

Nucleotide position	Nucleotide(s) in $P2^{VeroE6}$	Nucleotide change	Frequency in $P1^{Huh7.5}$ virus (%)	Frequency in $P5^{Huh7.5}$ virus (%)	Frequency in $P6^{Huh7.5}$ virus (%)	Amino acid change	Genomic region
7917	A	T	16.7	37.5	22.2	E→V	nsp3
11522	T	G	3.1	61.9	83.7	F→V	nsp6
11750	C	T	3.9	12.3	7.0	L→F	nsp6
16347	A	G	•	12.6	19.5	—	nsp13
19895	C	T	•	30.7	33.8	A→V	nsp15
20482	T	C	•	•	5.0	S→P	nsp15
20483	C	T	•	0.8	5.2	S→F	nsp15
21752	T	A	•	24.6	46.9	W→R	S
21762...21788	CTA...GTA	Δ	100	99.9	99.9	Δ9	S
22110	A	G	2.4	5.6	1.1	Q→R	S
22264	C	T	0.6	24.7	23.2	—	S
23014	A	C	92.4	98.7	99.7	E→D	S
23997	C	G	•	92.9	99.2	P→R	S
24424	A	C	3.2	93.1	98.3	Q→H	S
24983	T	G	•	6.7	5.9	L→V	S
26187	T	C	82.6	85.7	81.6	—	ORF3a
26333	C	T	1.0	14.8	20.9	T→I	E
28331	C	T	•	13.5	17.4	P→S	N

[a]The nearly full-length sequence of the virus grown in Huh7.5 cells (as described in Table 1) was obtained by NGS (cutoff of 5%). The sequence of the $P2^{VeroE6}$ virus is used as the reference, and the differences in the Huh7.5-recovered viruses are indicated. "Δ" refers to a deletion. The $P2^{VeroE6}$ virus refers to the stock pool of the second passage in Vero E6 cells. For the viruses recovered from Huh7.5 cells, the days used for sequencing were day 12 for $P1^{Huh7.5}$, day 3 (stock) for $P5^{Huh7.5}$, and day 4 for $P6^{Huh7.5}$. For more details, see Table 1.

consensus sequence of the adapted-SARS2 variant can be found in GenBank (accession no. MZ049598).

Adaptation of SARS-CoV-2 to efficient growth in Huh7.5 cells increases viability in unmodified Calu-1 and A549 but not Calu-3 cells. We reasoned that Huh7.5-adapted-SARS2 might overcome culture restriction in other human cell lines, including respiratory tract cell lines, which would be the most relevant infection model for culture studies. Both original-SARS2 and adapted-SARS2 were able to infect Calu-3 cells, and the obtained infectivity titers were not significantly different: the means (standard deviations) from two independent experiments were 4.1 (0.9) and 4.6 (1.6) $\log_{10}$ $TCID_{50}$/ml for original-SARS2 and adapted-SARS2, respectively. However, compared to original-SARS2, adapted-SARS2 exhibited a significant increase in the ability to infect Calu-1 cells, with a >2-log increase in infectivity titers (from 3.5 to 6.0 $\log_{10}$ $TCID_{50}$/ml) (Fig. 2A). Interestingly, adapted-SARS2 was able to efficiently infect A549 cells, with titers of 6.0 $\log_{10}$ $TCID_{50}$/ml, whereas original-SARS2 was confirmed to be nonviable in the A549 cell line (Fig. 2A). Albeit at lower levels than in Huh7.5 cells, we also detected CPE in Calu-1 and A549 cells infected with adapted-SARS2, for which no CPE was observed with original-SARS2 (Fig. 2B), indicating enhanced replication. Evidence for enhanced replication was also found by a higher intensity of antigen staining using an anti-spike protein antibody and an increased number of infected cells after infection of Calu-1 cells with adapted-SARS2 (Fig. 2C).

In addition, we also found that the viruses harvested from the persistently infected Vero E6 culture (day 42) (Fig. 1A) were able to efficiently infect A549 cells (Fig. 2C), with a titer of 3.7 $\log_{10}$ $TCID_{50}$/ml, a phenotype that was not shared by the virus recovered after serial passage in Vero E6 cells.

Importance of ACE2 and SR-B1 for the viability of original and adapted SARS-CoV-2 in various human cell lines. We found different cell-specific expression levels of ACE2 (Fig. 3A). Vero E6 cells exhibited the highest levels of ACE2 and were the most permissive cells for the original virus (Fig. 3B). However, in other cell types, permissiveness was not completely related to ACE2 levels. Calu-1 cells expressed ACE2 at levels comparable to those of Huh7.5 cells but were clearly less permissive to the original virus (Fig. 3B). We detected ACE2 expression in A549 cells albeit at lower levels, but no infection was possible even at a high multiplicity of infection (MOI), yet Huh7 cells

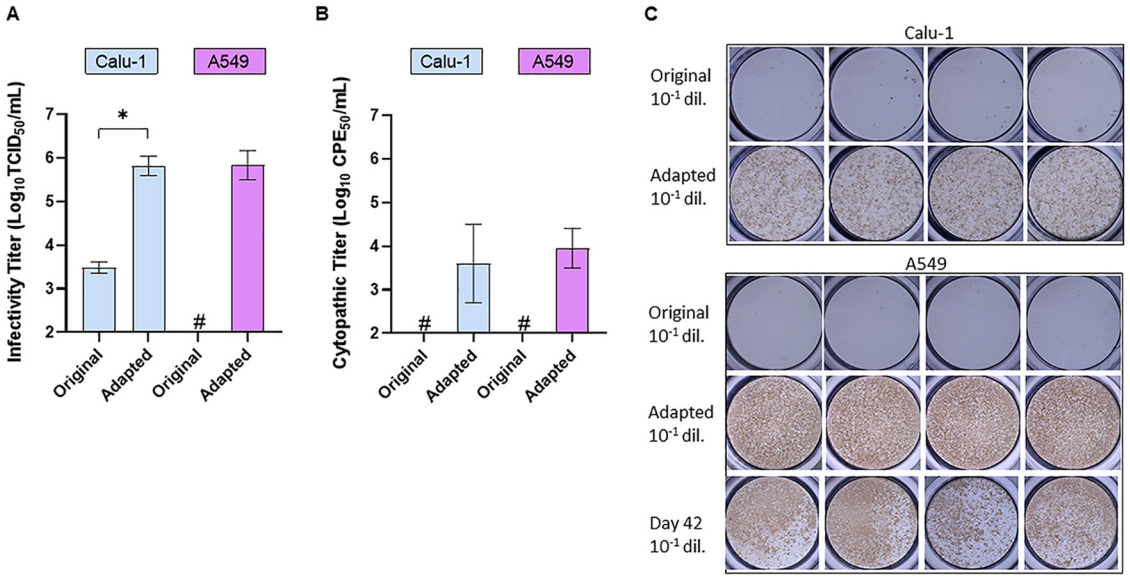

FIG 2 Adaptation of SARS-CoV-2 to Huh7.5 cells permits virus culture in human lung carcinoma Calu-1 and A549 cells. (A) Comparative infectivity titers of the original and adapted viruses in Calu-1 and A549 cells. Infectivity titers (log_{10} $TCID_{50}$ per milliliter) are shown on the *y* axis. For each cell line, results are based on 3 independent experiments with 4 replicates each. For the $P2^{VeroE6}$ (original) virus in A549 cells, none of the experiments yielded detectable titers (#). Bars represent the means and SEM for the different independent experiments. Statistical significance ($P < 0.05$ by an unpaired *t* test) is highlighted with an asterisk. (B) Comparative cytopathic effects of the original and adapted viruses in Calu-1 and A549 cells. Cytopathic effect titers (log_{10} CPE_{50} per milliliter) are shown on the *y* axis. Results are based on two independent experiments with 4 replicates each. CPE was below the detection limit in the two experiments with the original virus in both cell lines (#). (C) Visual comparative SARS-CoV-2 antigen staining of original and adapted viruses in Calu-1 cells (top) and of original, adapted, and day 42 (Vero E6) viruses in A549 cells (bottom), from representative $TCID_{50}$ assays.

were permissive to the virus despite also exhibiting low levels of ACE2. Blocking of ACE2 prevented infection of Vero E6 cells with original-SARS2 and, to a lesser extent, adapted-SARS2. However, in Huh7.5 cells, only infection with original-SARS2 was significantly prevented, whereas adapted-SARS2 was unaffected by ACE2 blocking at the tested antibody concentrations (Fig. 3C). In Calu-1 and A549 cells, ACE2 blocking did not have any effect on infection (Fig. 3C).

Scavenger receptor class B type 1 (SR-B1) was recently suggested to facilitate SARS-CoV-2 entry (21). Treatment of cells with the SR-B1 antagonist ITX5061, which inhibits the SR-B1 protein pathway (22), decreased the infectivity of both variants in a concentration-dependent manner in all cell types tested. Differences between original- and adapted-SARS2 were apparent only with 50 μM of inhibitor in Huh7.5 cells; however, both viruses were similarly inhibited in Vero E6 cells at all drug concentrations tested (Fig. 4A). Blocking SR-B1 also prevented infection with adapted-SARS2 in lung cells, most prominently in Calu-1 cells (Fig. 4A).

Differential antiviral activity of type I interferon against original and adapted viruses across cell types. The addition of interferon alpha 2b (IFN-α2b) resulted in a concentration-dependent antiviral effect on Vero E6, human hepatoma, and human lung cancer cells (Fig. 4B). Adapted-SARS2 was more responsive to IFN-α2b than original-SARS2 in both Vero E6 and Huh7.5 cells. When comparing the sensitivities of adapted-SARS2 to exogenous interferon treatment, the virus was more susceptible in Vero E6, Calu-1, and A549 than in Huh7.5 cells (Fig. 4B).

Susceptibility of cell culture-derived SARS-CoV-2 to neutralization by convalescent-phase COVID-19 plasma. To assess whether culture adaptation and, thus, the associated mutations affected sensitivity to neutralizing antibodies, plasma samples from 6 convalescent individuals with PCR-confirmed SARS-CoV-2 infection were used to neutralize both original-SARS2 and adapted-SARS2 in concentration-response assays in Vero E6 cells (Fig. 5A). No significant differences were observed when the combined

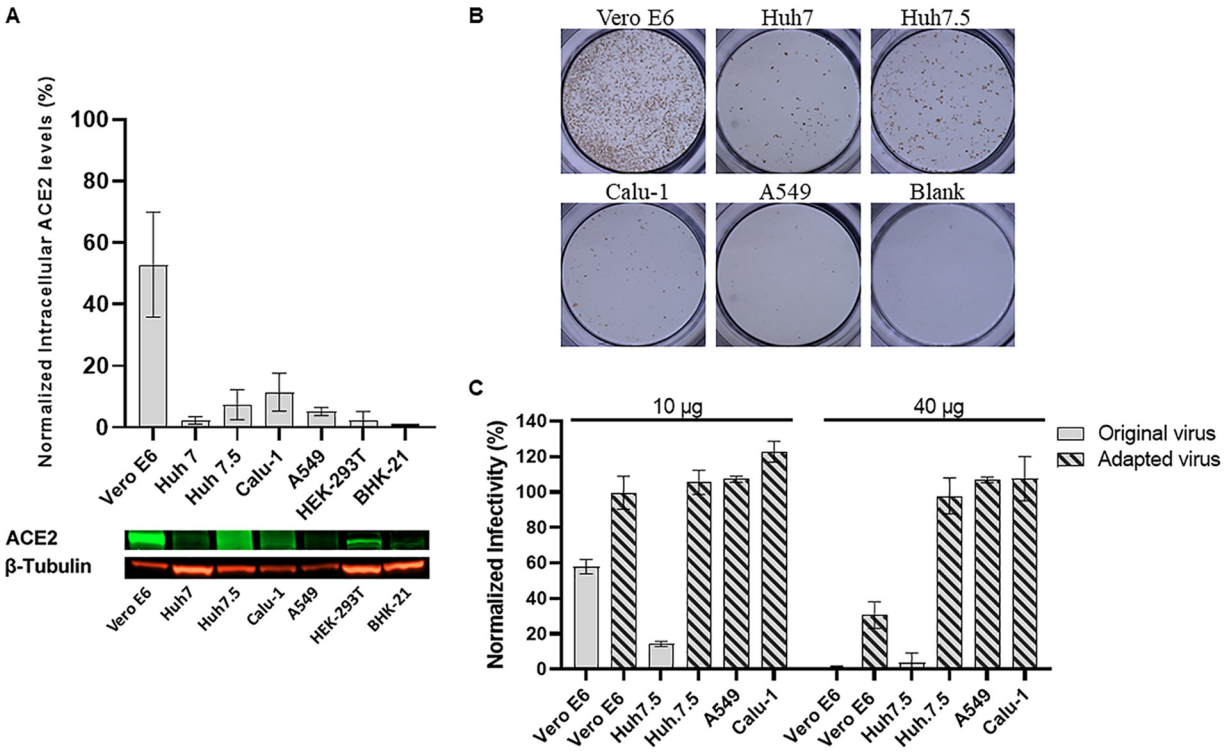

FIG 3 Correlation between ACE2 expression and the viability of original and adapted SARS-CoV-2 in different cell lines. (A) Graph showing intracellular ACE2 expression in the indicated cell lines assessed by Western blotting of ACE2. Values represent the fold amounts of ACE2 in each cell type relative to the levels detected in BHK-21 (baby hamster kidney) cells (black bar). Each gray bar represents the mean and standard deviation (error bars) from three independent experiments. An image of one of the three independent Western blots showing the bands corresponding to ACE2 (green) and the common housekeeping protein β-tubulin (red) is shown below the graph. (B) Representative image of cells infected with 100 μl of an undiluted stock of the original virus (MOI of 4 according to Vero E6). SARS-CoV-2 antigen staining was performed as indicated in the legends of Fig. 1D and Fig. 2C. No infected cells were detected in A549 cells. (C) Effect of ACE2 blocking using an anti-hACE2 antibody on SARS-CoV-2 infection for the different cell types. The *y* axis represents the percentage of the number of virus-positive cells normalized to nontreated controls, and bars show means and standard errors of the means from 7 and 4 replicates for 10 μg and 40 μg of ACE2-blocking antibody, respectively.

50% inhibitory dilution (ID_{50}) values obtained for all plasma samples were grouped according to the target virus ($P > 0.05$) (Fig. 5B).

Activity of remdesivir against original and adapted viruses in Vero E6 and Huh7.5 cells. Remdesivir was previously reported to inhibit SARS-CoV-2 in Vero (23–25) and human lung (Calu-3) (11) cells. Here, we found 50% effective concentration (EC_{50}) values of 1.5 μM in the concentration-response assays with original-SARS2 in Vero E6 cells (Table 3). Furthermore, we demonstrated that this drug displayed ~50-fold-higher activity against original-SARS2 in Huh7.5 cells (EC_{50} of 0.03 μM) (Table 3). For comparison, we found that remdesivir is a very potent inhibitor of different genotypes of HCV in Huh7.5 cells, with EC_{50} values of 0.08, 0.12, and 0.19 μM for genotypes 1, 2, and 3, respectively. Finally, we observed that remdesivir was very similarly active (<2-fold difference) against original-SARS2 and adapted-SARS2 when tested in Vero E6 or Huh7.5 cells (Table 3). Thus, the adapted virus represents a valid tool for the screening of SARS-CoV-2 polymerase inhibitors in cell culture.

Screening of the antiviral activity of a panel of NUCs in human cells using adapted SARS-CoV-2. Adapted-SARS2 facilitated drug testing in unmodified Huh7.5, Calu-1, and A549 cells. We focused our screening on NUCs previously shown to have an antiviral effect against HCV, including sofosbuvir (26), and broader-spectrum molecules such as remdesivir, galidesivir, favipiravir, and ribavirin.

Among the NUCs tested, only remdesivir and molnupiravir (EIDD-2801 prodrug of NHC) displayed a significant effect across human cells (Table 3), as previously described (27). Remdesivir was most active in Huh7.5 cells, with ~6-fold-lower EC_{50} values than in

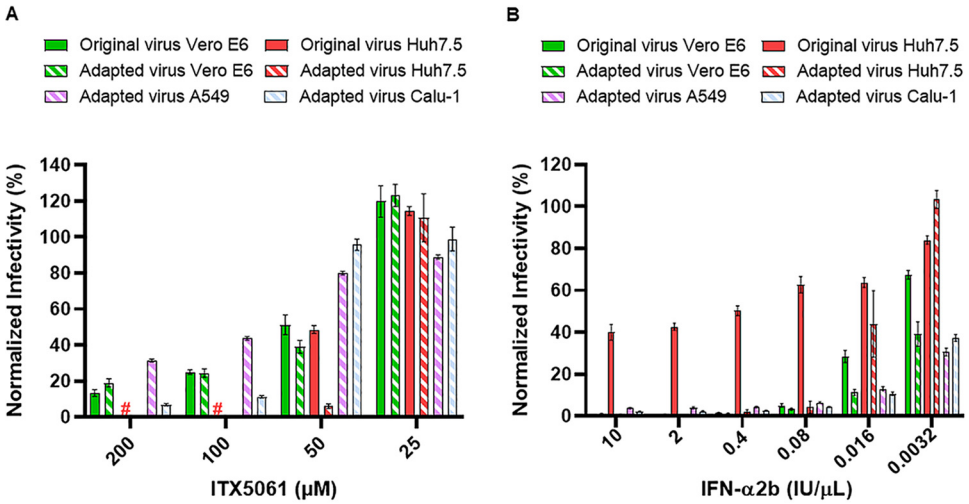

FIG 4 Dependence on SR-B1 and sensitivity to interferon of original and adapted SARS-CoV-2 in different cell lines. (A) Effect of treatment with the SR-B1 antagonist ITX5061 on SARS-CoV-2 infection. The *y* axis represents the percentage of the number of virus-positive cells normalized to nontreated controls, and bars show means and standard errors of the means from seven replicates. "#" indicates a lack of data as the corresponding concentrations of ITX5061 were cytotoxic in Huh7.5 cells. (B) Treatment with interferon alpha 2b. The *y* axis represents the percentage of the number of virus-positive cells normalized to nontreated controls, and bars show means and standard errors of the means from 6 replicates for Vero E6, Calu-1, and A549 cells and 3 replicates for Huh7.5 cells. In cases where the bar is not visible, the values were close to zero.

Calu-1 and A549 cells. Despite being less active in lung carcinoma than in hepatoma cells, remdesivir was still more potent in Calu-1 and A549 than in Vero E6 cells (>9-fold-lower EC_{50}). The opposite was observed for molnupiravir (Table 3), which was more active in A549 and Calu-1 cells (6- and 3-fold more active, with EC_{50}s of 1.3 μM and 2.7 μM, respectively) than in Huh7.5 cells (8.5 μM). Finally, galidesivir exhibited limited activity (Table 3), with a relatively high EC_{50} (>20 μM); the best inhibitory effect was observed in A549 cells. Other NUCs, including sofosbuvir, had no apparent activity (EC_{50} of >50 μM) in these human cell lines under our experimental conditions (Table 3).

DISCUSSION

In this study, we performed isolation of SARS-CoV-2 (isolate DK-AHH1) in Vero E6 cells and subsequent serial passage of the virus in human hepatoma cells (Huh7.5 clone) that led to cell culture adaptation of the virus with increased infectivity and cytopathic effect titers in both Vero E6 and Huh7.5 cells. Most importantly, human hepatoma cell culture adaptation significantly increased viral viability in lung carcinoma Calu-1 and A549 cells as well as in the parental Huh7 cell line, which do not efficiently support the replication and propagation of the original SARS-CoV-2 isolate. To our knowledge, the ability of the Calu-1 cell line to support SARS-CoV-2 replication and propagation has not been previously reported. The Calu-1 and A549 cell lines are widely available and well-characterized standards among the human lung carcinoma/alveolar cell lines used in cancer research (28, 29). Furthermore, the A549 cell line is also a model for the study of respiratory viruses such as respiratory syncytial virus and influenza virus (30, 31). The adapted virus might permit culture across additional human cell lines, a proposition that should be the topic of future investigations. We also demonstrated that the adapted virus is an efficient tool for the screening of putative SARS-CoV-2 antiviral compounds in human cells. Remdesivir, a known NUC with anticoronavirus activity, exhibited increased potency in human cells compared to Vero E6 cells, highlighting the importance of testing NUCs in the appropriate target cells.

The Huh7.5 cell line was originally selected to permit higher replication levels of HCV subgenomic replicons, and it has been of fundamental importance to the development of efficient culture systems for HCV (17, 18). Compared to the parental Huh7

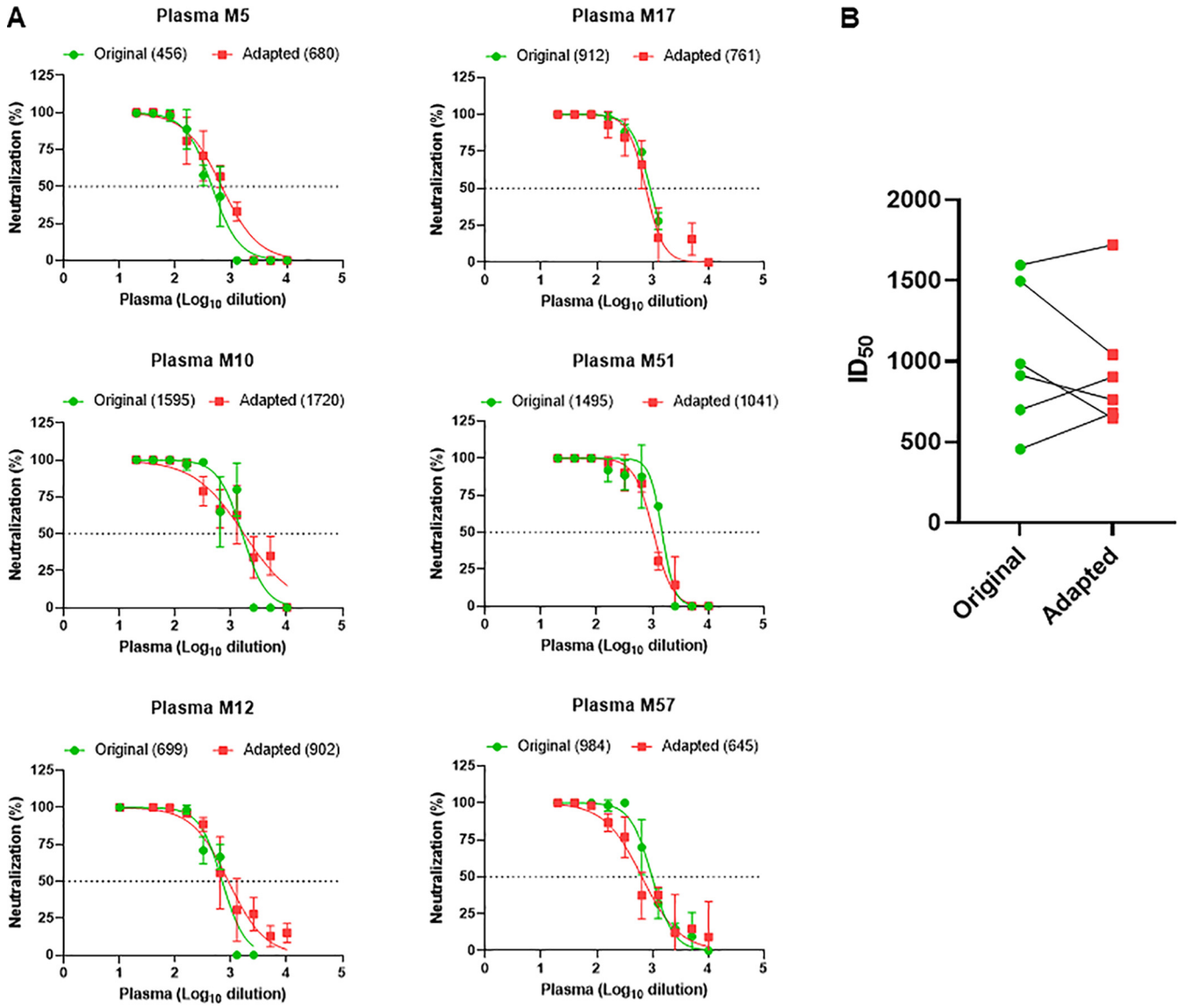

FIG 5 Neutralization of original and adapted SARS-CoV-2 variants. (A) Neutralization was analyzed for plasma samples obtained following recovery from COVID-19 in six individuals. Each graph shows the data obtained from a single experiment for each plasma sample against original and adapted viruses. The lines represent the nonlinear regression of virus inhibition compared to nontreated controls (*y* axis) in the different plasma dilutions (*x* axis). Bars represent the standard deviations from at least 3 replicates. The calculated 50% inhibitory dilution (ID_{50}) value for each virus variant is shown in parentheses. The dotted line highlights the 50% neutralization level. All infections were performed at an MOI of 0.01 except for infection with the original virus in the neutralization of plasma sample M57, which was performed at an MOI of 0.02. (B) Comparison of the ID_{50} values between the two groups (original and adapted variants). No significant differences were found using a Wilcoxon-Mann-Whitney test ($P > 0.05$).

cell line, the Huh7.5 clone exhibits a mutation that inactivates retinoic acid-inducible gene I (RIG-I), an interferon-inducible cellular helicase involved in the type I interferon response, one of the features that has been correlated with increased permissiveness to HCV replication (32). Interestingly, Huh7 cells are highly susceptible and permissive to SARS-CoV, which induces lytic and productive infections (33). A previous study demonstrated that SARS-CoV-2 is more sensitive to type I interferons than SARS-CoV (34), and this enhanced susceptibility could be one of the reasons why SARS-CoV-2 viability in cell culture is high in Vero cell lines, which lack genes encoding type I interferons (35). This could also partially explain our finding that the virus is more viable in Huh7.5 than in Huh7 cells. The increased IFN-α2b susceptibility found in the adapted virus supports the involvement of interferon responses in culture adaptation, although the mechanism merits further investigation.

TABLE 3 Anti-SARS-CoV-2 activity of a panel of nucleos(t)ide analogs in different cells for original and adapted viruses[a]

	EC_{50} (μM)					
	Original virus		Adapted virus			
Nucleos(t)ide analog	Vero E6	Huh7.5	Vero E6	Huh7.5	Calu-1	A549
Remdesivir	1.5	0.03	2.9	0.05	0.29	0.31
Molnupiravir	ND	ND	ND	8.5	2.7	1.3
GS-6620	ND	ND	ND	>25	>25	>25
Galidesivir	ND	ND	ND	48	58	24
Sofosbuvir	ND	ND	ND	>50	>50	>50
Uprifosbuvir	ND	ND	ND	>50	>50	>50
Valopicitabine	ND	ND	ND	>50	>50	>50
Mericitabine	ND	ND	ND	>50	>50	>50
Ribavirin	ND	ND	ND	>50	>50	>50
Favipiravir	ND	ND	ND	>50	>50	>50

[a]For each compound, the antiviral activity in Vero E6, Huh7.5, Calu-1, or A549 cells is indicated by 50% effective concentration (EC_{50}) values (micromolar). These values were inferred from concentration-response curves based on 6 replicates (GS-6620) or 3 replicates (all other compounds). All compounds were tested at noncytotoxic concentrations as described in Materials and Methods. ">50" or ">25" indicates that the maximum concentration tested was 50 or 25 μM and that no viral inhibition reaching 50% was observed at this concentration. ND, not done.

Cell culture adaptation in Huh7.5 cells correlated with a significant accumulation of substitutions in the genomic region coding for the spike protein, which could mediate enhanced infectivity. Likewise, we found that regular culture in Vero E6 cells, used worldwide for experimental studies of SARS-CoV-2, results in a significant accumulation of changes in the spike protein, suggesting that this region is under selective pressure in cell culture. More interestingly, the spike protein appears to be under strong selection *in vivo* as well, as multiple spike mutations can be found in variants infecting humans, including changes at position E484 and, to a lesser extent, at positions P812 and Q954 (36), which are involved in the culture adaptation reported here.

The first complete change observed during culture adaptation in Huh7.5 cells was the deletion of the IHVSGTNGT loop in the N-terminal domain of S. This deletion leads to the removal of amino acid N74, which is N-glycosylated (37), and interestingly, this loop is not present in SARS-CoV, but it is found in Middle East respiratory syndrome coronavirus (MERS-CoV) (Fig. 6A and B). Smaller deletions within this region (Δ69/Δ70) were recently reported in patients in Europe and have been linked to increased transmissibility of SARS-CoV-2 in the United Kingdom (38). However, to date, no animal transmission studies have been performed to support these observations. Moreover, a study estimating the transmissibility of circulating variants of SARS-CoV-2 (based on phylogenetic indexes) found no convincing evidence of increased viral transmission of several emerging variants (36). More studies involving animal models are needed to establish a direct relationship between emerging spike mutations and enhanced transmissibility.

E484D, which appeared early during culture adaptation in Huh7.5 cells and during long-term infection of the original inoculated Vero E6 culture, is located in the receptor binding domain and interacts with K31 in the ACE2 receptor (39). Noticeably, an *in silico* study of E484D predicted a higher ACE2 binding affinity that could render a more infectious SARS-CoV-2 variant (40), which is further supported by our ACE2-blocking experiments in which more ACE2 antibody is needed to decrease the infectivity of the adapted virus. Indeed, mutation E484D, which was the only common spike mutation in the two viruses that recapitulated the entire virus life cycle in unmodified A549 cells (adapted-SARS2 and the virus harvested on day 42 after inoculation of Vero E6 cells), might be a major contributor to culture adaptation in human cells, possibly through an increased binding affinity for ACE2. Nevertheless, as adapted-SARS2 was still more efficient in replicating and propagating in human cells than the Vero E6 day 42 virus, other mutations found in adapted-SARS2 might significantly contribute to this

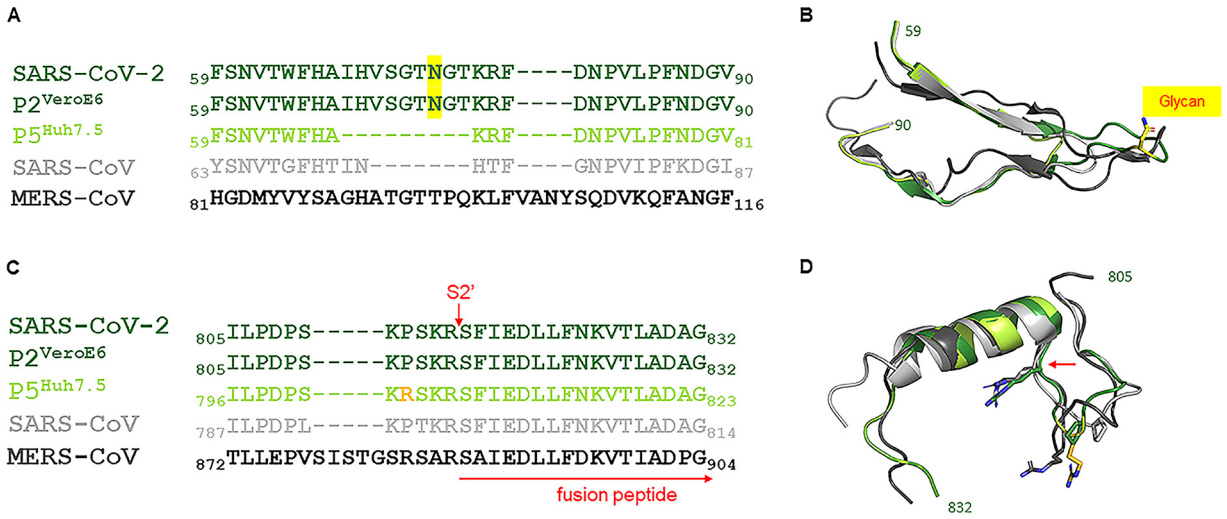

FIG 6 Structural overview of changes found in the spike protein of SARS-CoV-2 after culture adaptation in Huh7.5 cells. A multiple-sequence alignment of the partial spike protein sequences of SARS-CoV-2 (GenBank accession number MN908947), $P2^{VeroE6}$ (original) virus, $P5^{Huh7.5}$ (adapted) virus, SARS-CoV (GenBank accession number AY278741), and MERS-CoV (GenBank accession number JX869059) was carried out using MUSCLE software (78). (A) Alignment of the area containing the N-terminal 9-amino-acid deletion in adapted viruses, which corresponds to the protein-specific positions indicated with numbers. The SARS-CoV-2 sequences are shown in green, with the N74 glycosylation site highlighted in yellow; the SARS-CoV sequence is in gray; and the MERS-CoV sequence is in black. (B) Structural alignments of SARS-CoV and MERS-CoV spike proteins (PDB accession numbers 5X58 [79] and 6Q04 [80], respectively) to the SARS-CoV-2 spike protein (PDB accession number 7JJI [81]) using PyMOL (82) with the same parts of the sequences as the ones shown in panel A. The same color coding as in panel A is used. N74 is shown as sticks in SARS-CoV-2, and an attached glycan is illustrated schematically. The structure for the adapted virus was generated from the SARS-CoV-2 structure by introducing the deletion and modeling the loop closure ("HAKRFD") with ModLoop (83). (C) Alignment of the area around the S2′ cleavage site (indicated with a red arrow). The observed P812R mutation is highlighted in orange. (D) Structural alignments with the same parts of the sequences as the ones shown in panel C. Structures were generated as explained above for panel B using the same PDB entries except for the SARS-CoV spike protein (PDB accession number 5XLR [84]). Residues that align with P812 and R815 in SARS-CoV-2 are represented as sticks. A part of the MERS-CoV sequence ("SISTGSRS") was modeled using ModLoop (83), as the residues were missing in the experimental structure. The S2′ cleavage site is indicated with a red arrow.

phenotype, for instance, mutation P812R, which emerged only during the latest passages, when the virus exhibited maximum infectivity. P812 is positioned near the S2′ cleavage site, and this proline is also present in SARS-CoV; however, at that position, R is present in MERS-CoV (Fig. 6C and D). P812R changes the sequence "PSKR" to "RSKR," which corresponds to the furin consensus cleavage motif ("RX[K/R]R") (41, 42); thus, a putative second furin cleavage site could have emerged at the S2′site. Whether the emergence of a new furin cleavage motif near the S2′ site plays a role in culture adaptation by increasing membrane fusion and, therefore, infectivity, as seen in SARS-CoV, warrants further investigation (43, 44). Similarly, it was found that cell culture adaptation (Vero cells) of the coronavirus infectious bronchitis virus (Beaudette strain) led to the acquisition of a mutation in the S protein, creating a novel furin site downstream of the S1/S2 site that was implicated in entry and syncytium formation in Vero cells (45). On the other hand, deletions in the S1-S2 furin cleavage site have been found during culture adaptation of SARS-CoV-2 in Vero E6 cells (25, 46). Finally, Q954H was present at a low frequency in P1 but increased significantly in later passages in Huh7.5 cells, consistent with the maximum increase in viral infectivity. Residue Q954 is located in heptad repeat 1 (HR1) within the S2 subunit, which undergoes conformational rearrangements from prefusion to postfusion states. Thus, the Q954H change may contribute to increased infectivity by enhancing fusion activity, in a manner similar to that suggested for other HR1 mutations (47). The specific role of the spike mutations described here in culture adaptation merits future investigations involving reverse genetics and possibly knockout/knockdown of ACE2 and SR-B1.

As described here by us, and elsewhere by others, the A549 cell line is refractory to infection with SARS-CoV-2 (48). For both SARS-CoV and SARS-CoV-2, exogenous ACE2 expression supports enhanced virus viability in A549 cells (14, 49). However, natural

ACE2 expression in A549 cells was reported by other groups (50, 51), and here, we find limited but consistently detectable expression of ACE2 in this cell type. Moreover, we found no direct association between ACE2 expression and the viability of the original virus in the different cell types, indicating that ACE2 expression might not be the only factor contributing to susceptibility/permissiveness in culture. Additional receptors involved in SARS-CoV-2 entry in culture have been recently reported (21, 52, 53); thus, entry might involve complex interactions between the spike and several coreceptors.

Another entry host factor for SARS-CoV-2 is transmembrane protease serine 2 (TMPRSS2) (41). Vero E6 cells expressing TMPRSS2 permit enhanced isolation of SARS-CoV-2 (13), and TMPRSS2 has also been described as a host entry factor for SARS-CoV, specifically isoform 1 of the protein, directly linked to the activation of the spike protein (54). This isoform was found to be expressed in permissive cells (such as Calu-3) but was lacking in refractory A549 cells (54). TMPRSS2 is not expressed in Huh7 cells either (55), which could further account for the poor viability of the original virus in A549 and Huh7 cells. The acquisition of the furin cleavage site by substitution P812R, which could compensate for a putative low level of activation of spike due to inadequate TMPRRS2 expression, might represent another mechanism of culture adaptation meriting further investigation.

Adapted-SARS2 facilitated the screening of polymerase inhibitors in different cell types. In agreement with the results of others, we found that the NUCs remdesivir and molnupiravir exhibited increased activity in human cells compared to Vero cells (11, 27). For remdesivir, maximum activity was observed when using human hepatoma cells, as expected since this compound originated from the HCV antiviral program and, like sofosbuvir, is masked by a McGuigan prodrug moiety, leading to a significant accumulation of the active compound in the liver (56). In the present study, we also show a proof of concept of the potent inhibitory effect of remdesivir against cell culture infectious recombinants of HCV genotypes 1, 2, and 3 with EC_{50} values lower than those routinely obtained with sofosbuvir (57–60). For molnupiravir, maximal activity against SARS-CoV-2 was observed in lung cells, in agreement with previous studies showing high activity of the drug in human airway epithelia infected with influenza virus (61). The obtained EC_{50} values for remdesivir in Vero E6 and Calu-1 cells were very similar to those reported previously for Vero and Calu-3 cells, respectively (11). However, for molnupiravir (oral bioavailable prodrug of NHC), the EC_{50} values in Calu-1 and A549 cells were higher than the previously reported NHC values in Calu-3 cells (27), which could be explained by the use of the prodrug in the present study.

Our investigated panel of NUCs included molecules that had been previously shown to inhibit the virus but also compounds that had been proposed as drug candidates. Strikingly, no analogs other than remdesivir and molnupiravir showed a significant inhibitory effect under our experimental conditions, including sofosbuvir, which had been the subject of extensive *in silico* investigations (62) and was found to cause chain termination of the SARS-CoV-2 polymerase *in vitro* (63). It is important to acknowledge that studies assessing only the incorporation and chain termination of nucleotide analogs as antiviral strategies against coronaviruses lack a complete overview of the structural requirements for viral replication, including the role of the nsp14 exonuclease in excising these molecules, which remdesivir overcomes (64). Favipiravir, a broad-spectrum antiviral with a mechanism of action similar to that of molnupiravir, exhibited no antiviral effect under our experimental conditions but contrarily showed anecdotal activity in patients (65). However, proper randomized trials are needed to confirm these findings.

The broad-spectrum NUC galidesivir (66) exhibited a detectable inhibitory effect against SARS-CoV-2 in human lung carcinoma cells but significantly lower activity than remdesivir and molnupiravir. In light of the detectable inhibitory effect, it could be relevant to test the efficacy of this drug in primary airway cultures and in longer-term treatment assays where multiple doses of the drug are added to the culture to further elucidate the potential antiviral use of this compound.

We demonstrated the equivalent activity of remdesivir against original-SARS2 and adapted-SARS2 despite the latter exhibiting multiple changes in the genome. Since these changes were concentrated in the S protein and not in the nsp12 protein, which is the main target of NUCs, adapted-SARS2 represents an excellent tool to study this drug class in human cells. Thus, emerging mutations in the S protein are not likely to affect the susceptibility of the virus to relevant polymerase inhibitors used in the clinic, such as remdesivir, which is important information in light of the current propagation of spike mutants worldwide.

However, the spike mutations present in adapted-SARS2 could potentially interfere with entry processes, and therefore, this experimental system might not be an optimal tool for the screening of entry/fusion inhibitors. Despite this, compared to original-SARS2, adapted-SARS2 showed an identical neutralization susceptibility to convalescent-phase COVID-19 plasma and could be effectively blocked by an SR-B1 antagonist that can be used in the clinic.

Mutation E484D very often emerges during cell culture of SARS-CoV-2 (in both Vero E6 and human cells), versus E484K, which has been found in infected individuals, usually combined with N501Y. A recent study showed decreased susceptibility to neutralization from COVID-19 convalescent-phase plasma and SARS-CoV-2 vaccine sera of the South African (B.1.351) SARS-CoV-2 variant, which harbors several spike protein mutations, including E484K (67). It is important to highlight that this phenotype is not shared by culture-adapted variants with E484D, as demonstrated here; thus, extensive reverse-genetics studies will be needed to elucidate which positions and residues are involved in viral immune evasion *in vivo*.

Although the cell culture model developed here does not necessarily represent a relevant translational system to study the pathogenesis or transmissibility of viruses *in vivo*, it can be a very useful tool for the preclinical characterization of novel antiviral molecules that, combined with efficient vaccines, will be essential to prevent deaths and better control current and future pandemics.

MATERIALS AND METHODS

Cell culture experiments. All experiments in this study were performed with a novel isolate of SARS-CoV-2 (SARS-CoV-2/human/Denmark/DK-AHH1/2020), under biosafety conditions in agreement with Danish regulations and with permission from the Danish authorities. Initial culture of SARS-CoV-2_DK-AHH1 was performed in African green monkey kidney cells (Vero E6). Residual nasopharyngeal sample material was obtained after clinical diagnosis of COVID-19 (SARS-CoV-2 threshold cycle [C_T] value of 14 in a reverse transcription-PCR [RT-PCR] assay [68]) and irreversible anonymization. For inoculation, 30 μl of the diluted sample was added to 100,000 Vero E6 cells seeded in 12-well plates, 24 h prior to infection, at a final volume of 1 ml. For the initial inoculation experiment, Vero E6 cells were cultured in Dulbecco's modified Eagle's medium (DMEM) (high glucose, GlutaMAX, and pyruvate; Invitrogen) supplemented with 10% fetal bovine serum (FBS; Sigma) and antibiotic-antimycotic (100 U/ml of penicillin, 100 μg/ml of streptomycin, and 0.25 μg/ml of amphotericin B; Gibco) and kept at 37°C in a humidified incubator with 5% CO_2. This culture was maintained for over a month, consistently showing a high frequency of SARS-CoV-2 antigen-positive cells. Afterward, all experiments in Vero E6 cells were performed with DMEM supplemented only with 10% FBS and a penicillin-streptomycin mix (100 U/ml penicillin and 0.1 mg streptomycin/ml; Sigma). The culture was visually inspected under an inverted light microscope, and the supernatant was harvested daily and stored at −80°C. A first viral passage from the original inoculated culture was performed with 0.5 ml of the harvested supernatant from day 2 postinoculation in naive (noninfected) Vero E6 cells in a T-25 flask with 10^6 cells, with a final volume of 4 ml (MOI of ~0.02). Two independent second passages were performed with supernatants harvested at passage 1 day 2 (MOI of ~0.9) and day 3 (MOI not determined). For that purpose, 1.5 ml of the first-passage supernatant was used to infect 5×10^6 cells (final volume of 30 ml). A viral stock was prepared by pooling the filtered supernatant (0.45-μm filter; Sartorius) from the samples harvested at days 2 and 3 from both second passages (total of 120 ml), aliquoted, and stored at −80°C.

Human hepatoma (Huh7 and Huh7.5), HEK-293T, BHK-21, and Calu-1 cells (Sigma) were cultured in DMEM (high glucose, GlutaMAX, and pyruvate; Invitrogen, Thermo Fisher) supplemented with 10% fetal bovine serum (Sigma), 100 U/ml penicillin, and 0.1 mg streptomycin/ml (Sigma) and maintained at 37°C in a humidified incubator with 5% CO_2. A549 cells (Sigma) were cultured under the same conditions but with Ham's F-12K (Kaighn's) medium (Gibco, Thermo Fisher) supplemented with 10% fetal bovine serum and antibiotics. Calu-3 cells were cultured under identical conditions but using supplemented Eagle's minimum essential medium. Culture of HCV was performed as previously described with genotype 1a strain TNcc, genotype 2a strain J6/JFH1, and genotype 3a strain DBN3acc (57, 58, 69).

TABLE 4 Primers used for SARS-CoV-2 genome amplification procedures[a]

Target and primer	Sequence (5′–3′) or description
Amplicon 1, nt 1–6171	
RT primer	GCCACCACATCACCATTTA
PCR forward primer	ATTAAAGGTTTATACCTTCCCAGGTAACAAAC
PCR reverse primer	GCCACCACATCACCATTTAAGTCA
Amplicon 2, nt 6108–11945	
RT primer	ACTGGACACATTGAGCC
PCR forward primer	AGAAACCTGCTTCAAGAGAGCTT
PCR reverse primer	ACTGGACACATTGAGCCCACA
Amplicon 3, nt 11796–17904	
RT primer	ACAAGAGTGAGCTGTTTCA
PCR forward primer	TGTTGGGTGTTGGTGGCAAA
PCR reverse primer	ACAAGAGTGAGCTGTTTCAGTGG
Amplicon 4, nt 17832–23916	
RT primer	ACTTGTGCAAAAACTTCTTGG
PCR forward primer	TGTTGATTCATCACAGGGCTCAGA
PCR reverse primer	ACTTGTGCAAAAACTTCTTGGGTG
Amplicon 5, nt 23854–3′ end	
RT primer	Anchored oligo(dT)$_{20}$ (Invitrogen, USA)
PCR forward primer	CCGTGCTTTAACTGGAATAGCTGT
PCR reverse primer	GTCATTCTCCTAAGAAGCTATTAAAATCACATG
5′ UTR	
RT primer	TAAGCCACTGGTATTTCGCC
Template switch oligonucleotide	/5InvddT/GTCGCACGGTCCATCGCAGCAGTCACArGrG+G
PCR forward primer	GTCGCACGGTCCATCGCAGCAGTC
PCR reverse primer	GTGTCTCACCACTACGACCGTT
3′ UTR	
RT primer	GACCACGCGTATCGATGTCGACTTTTTTTTTTTTTTTV[b]
PCR forward primer	TGGATGACAAAGATCCAAATTTCAAAGA
PCR reverse primer	GACCACGCGTATCGATGTCGAC

[a]RT (reverse transcription) and PCR primers (forward and reverse) for each amplicon covering the nearly full-length PCR strategy (a single RT reaction was performed by pooling all 5 RT primers, which served as the template for each of the independent PCRs generating the 5 overlapping amplicons) and the ends of the untranslated regions (UTRs) are shown. Nucleotide numbering is according to the Wuhan-Hu-1 isolate (GenBank accession number NC_045512.2). RT and PCR primers for the determination of the 3′ UTR were obtained from Sigma. The remaining primers were obtained from TAG Copenhagen. 5InvddT refers to 5′ inverted dideoxy-T.
[b]V is A, C, or G.

Serial passage of SARS-CoV-2 in Huh7.5 cells. A total of six passages were conducted in Huh7.5 cells. Passages were performed by inoculating 10^6 naive cells (seeded in a T-25 flask) with a 1/10 dilution of the P2^{VeroE6} virus (P1) or with 0.5 ml of the supernatant for subsequent passages. The fifth passage was carried out in T-175 flasks (approximately 5 million cells were seeded) for the production of a viral stock.

Determination of viral titers. Infectivity titers were expressed as 50% tissue culture infectious doses ($TCID_{50}$) per milliliter. $TCID_{50}$ assays were performed in 96-well plates by infecting cells with 100 μl of 10-fold serially diluted virus-containing supernatants, in quadruplicates, followed by immunostaining of the SARS-CoV-2 spike protein (as described below) at 72 h postinfection. The presence or absence of infected cells in each replicate was scored and used to determine the $TCID_{50}$ per milliliter based on calculations obtained by the Reed and Muench method (as described in *Fields Virology*, 5th ed. [70]).

A CPE assay to determine the 50% cytopathic effect titer (CPE_{50}) per milliliter was developed under conditions similar to those for the infectivity assay, infecting cells with 100 μl of 10-fold dilutions of virus-containing supernatants, in quadruplicates. CPE was assessed at 72 h postinfection with the viral ToxGlo assay (Promega) according to the manufacturer's instructions. Relative light units (RLU) obtained for each infected well were normalized to the RLU of noninfected controls (100% cell normality or cell viability), values below 90% were considered positive for CPE, and the Reed and Muench method was used to calculate the titer as $\log_{10}$ CPE_{50} per milliliter. The assay was validated by correlating titer values obtained with the viral ToxGlo assay with visual inspections of the cells under a light microscope in

multiple assays. Graphical representations and statistical analyses were performed using GraphPad Prism 8 (GraphPad Software).

Sequencing of SARS-CoV-2. Viral sequencing of SARS-CoV-2 recovered from the original clinical specimen and from all cell culture-derived supernatants was performed in an identical manner with next-generation sequencing (NGS) of nearly full-length genomes from 5 overlapping amplicons in each pool. The methodologies for RNA extraction, generation of cDNA by reverse transcription (RT), and amplification of these overlapping amplicons were adapted from existing protocols for the amplification of the complete open reading frame of HCV (71). Specific SARS-CoV-2 primers can be found in Table 4. Determination of the sequences of the 5′ UTR of the original clinical specimen and of the cell culture-recovered $P2^{VeroE6}$ viruses was done using a template-switching RT method and reagents from New England BioLabs, following the manufacturer's guidelines. Gene-specific RT primers can be found in Table 4. The sequence of the 3′ UTR was determined by RT-PCR with an oligo(dT) anchor primer (Sigma) as described previously (72), using primers shown in Table 4. NGS analysis was performed as described previously (73), with minor modifications. In short, reads were trimmed from PCR primer sequences at the 5′ end by Cutadapt (74) to remove the bias of the 5′-overlapping amplicons. Next, reads were mapped to the appropriate SARS-CoV-2 reference sequence. Subsequently, consensus and low-frequency single nucleotide polymorphism (SNP) and insertion/deletion (indel) calling was performed.

Immunostaining of SARS-CoV-2-infected cell cultures. Following different assays, 96-well plates with confluent cell layers were fixed, and the virus was inactivated by immersion in 100% methanol (Merck) for 20 min. Cells were washed twice with PBST (phosphate-buffered saline [PBS] containing 0.1% Tween 20), followed by incubation with 3% H_2O_2 for 10 min to block endogenous peroxidase activity and washing twice with PBST. Cells were then incubated with primary SARS-CoV-2 spike chimeric monoclonal antibody (catalog number 40150-D004; Sino Biological) diluted 1:5,000 in PBS with 1% bovine serum albumin and 0.2% skim milk powder (PBSK) overnight at 4°C. Afterward, cells were washed twice with PBST followed by a 1-h incubation with $F(ab')_2$ goat anti-human IgG Fc cross-adsorbed secondary antibody conjugated to horseradish peroxidase (HRP) (catalog number A24476; Invitrogen), diluted 1:2,000 in PBSK. Cells were washed twice with PBST, and single infected cells were visualized with 3, 3′ diaminobenzidine tetrahydrochloride (DAB) substrate (catalog number BS04-110; Immunologic) and counted automatically by an ImmunoSpot series 5 UV analyzer (CTL Europe GmbH), as previously described for the focus-forming unit assays developed to study HCV in culture (75, 76). Examples of the immunostaining experiment outputs (images) can be seen in Fig. 1D, Fig. 2C, and Fig. 3B.

Treatment assays. Antivirals were obtained from Acme Bioscience and reconstituted in dimethyl sulfoxide (DMSO). For each drug tested, cytotoxicity assays were performed in the different cell types studied using the Cell Titer AQueous One solution cell proliferation assay [3-(4,5-dimethylthiazol-2-yl)-5-(3-carboxymethoxyphenyl)-2-(4-sulfophenyl)-2H-tetrazolium (MTS) assay; Promega]. The 50% cytotoxic concentration (CC_{50}) (micromolar) was calculated by regression analysis. In brief, cells were seeded in 96-well plates, and drug dilutions were added the next day, in triplicates. At 24, 48, or 72 h postinfection (depending on the assay type), the MTS reagent was added, and the absorbance was measured after 1 h of incubation at 37°C. The results of treated wells were normalized to those of nontreated controls, and the percentage of cell viability was plotted against the $\log_{10}$ of the drug concentration, followed by nonlinear regression ($y = \text{bottom} + (\text{top} - \text{bottom}) / \{1 + 10^{[(\log CC_{50} - x) \times \text{Hill slope}]}\}$) using GraphPad Prism 8. All treatments shown in this study were conducted at noncytotoxic concentrations (defined as cell viability of ≥75%).

To explore the overall antiviral activity of drug candidates (drug potency), cells were seeded in 96-well plates; the next day, 50 μl of virus (at a specific MOI that led to robust infection of all nontreated control wells, depending on the cell type) and 50 μl of drug (different concentrations as indicated) were added, and the cells were incubated for 72 h or, alternatively, 48 h. After incubation, the plates were processed for SARS-CoV-2 S-protein immunostaining as described above. The analysis was performed by counting the numbers of antigen-positive cells, which were then normalized to the nontreated controls (after subtraction of the background levels obtained from noninfected wells), and 50% effective concentration (EC_{50}) values were obtained after nonlinear regression, as stated above. Treatment of HCV was performed in Huh7.5 cells as previously described (57–60).

Receptor blocking assays. ACE2 blocking was performed with an ACE2-specific antibody (catalog number AF933; R&D Systems), whereas the antagonist ITX5061 (purchased from Acme Bioscience) was used to inhibit SR-B1. Cells were seeded in 96-well plates 2 days prior to the assay. Cells were treated with each compound during 3 h prior to infection; afterward, the different viruses were added (at an MOI depending on viral viability in each cell type, sufficient to perform reliable counting of infected cells at the indicated time points), and cultures were incubated for 24 h and processed for viral immunostaining as described above.

Fluorescent Western blotting. Cell lysates were prepared using M-PER extraction buffer (Thermo Fisher) supplemented with Halt protease and phosphatase inhibitors (Thermo Fisher), according to the manufacturer's recommendations. Briefly, cells were washed twice with cold PBS, lysed in buffer for 30 min, and centrifuged for 15 min at maximum speed at 4°C, and the supernatants were collected and stored at −20°C for subsequent analysis. The total protein concentration was determined using a bicinchoninic acid (BCA) assay (Pierce) according to the manufacturer's recommendations. Polyacrylamide gel electrophoresis (PAGE) was performed using NuPAGE Bis-Tris 4 to 12% gels (Thermo Fisher), and separated proteins were blotted on Immun-Blot low-fluorescence polyvinylidene difluoride (PVDF) membranes (Bio-Rad). Membrane blocking was carried out in Rockland blocking buffer for fluorescent Western blotting (Rockland Immunochemicals) overnight, followed by primary staining in the same buffer using goat anti-ACE2 antibody at 1:1,000 (catalog number AF933; R&D Systems) and mouse-anti-β-tubulin antibody at 1:2,000 (catalog number MA5-16308;

Thermo Fisher). Secondary staining was done with donkey anti-goat antibody conjugated to Alexa Fluor 488 and goat anti-rabbit antibody conjugated to Alexa Fluor Plus 647 (Thermo Fisher). Imaging was performed with a Chemidoc MP system (Bio-Rad) equipped for multicolor Western blotting. Protein band quantification was performed with ImageLab 6.1 (Bio-Rad), using β-tubulin bands for normalization.

Neutralization assay. Plasma was obtained from 6 convalescent COVID-19 individuals with confirmed SARS-CoV-2 infection during April to September 2020 from the Clinical, Virological, and Immunological COVID-19 (CVIC) study at Hvidovre Hospital (Capital Region's Committee on Health Research Ethics, project identifier H-20025872, Data Protection Agency [Pactius] journal number P-2020-357). Therefore, these individuals were not exposed to any of the newly emerging SARS-CoV-2 variants. Plasma was heat inactivated at 56°C for 30 min and diluted 1/10 in PBS (Sigma-Aldrich). From this initial dilution, 2-fold serial dilutions (a total of 10 dilutions) were prepared for the assay and mixed 1:1 with the corresponding virus at an MOI of 0.01 (except in one case in which the MOI was 0.02, as indicated in the Fig. 5A legend). Plasma and virus were mixed and incubated at room temperature for 1 h. A positive-control neutralizing antibody (catalog number 40592-MM57; Sino Biological) as well as a negative pool of healthy plasma (final dilution of 1/20) were used as controls for each assay. After incubation, 100 μl of the plasma-virus mixture was added to 10,000 Vero E6 cells (seeded 1 day prior to the experiment in BioCoat 96-well poly-D-lysine-coated plates [Corning]) in quadruplicates and incubated for 48 h. Following incubation, the cells were fixed and stained as described above with the following modifications: a mouse-derived anti-spike protein primary antibody (catalog number 40592-MM57; Sino Biological) (diluted 1:5,000 in PBSK) was used for primary staining, and an anti-mouse secondary Ab conjugated with HRP (catalog number NA931V; GE Healthcare) (diluted 1:5,000 in PBSK) was used for secondary staining. Spots were counted as described above. Outliers of quadruplicates were determined using a modified Z-score system as previously described (77) and were excluded from further analysis; in all cases, at least 3 replicates could be included. Neutralization titration curves were plotted and analyzed using GraphPad Prism 8 (GraphPad Software), and the 50% inhibitory dilution (ID_{50}) value was calculated using the following equation: $y = 100/\{1+10^{[(\log IC_{50}-x)\times \text{Hill slope}]}\}$. Combined ID_{50} values grouped according to variant were compared using a Wilcoxon-Mann-Whitney test, and statistical significance was determined as a P value of less than 0.05.

Data availability. Virus genomes have been deposited in GenBank under accession no. MZ049597 and MZ049598.

ACKNOWLEDGMENTS

We thank Bjarne Ørskov Lindhardt (Hvidovre Hospital) and Carsten Geisler (University of Copenhagen) for their support of these studies and Anna-Louise Sørensen, Susanne Ruszczycka, Pia Pedersen, Signe Villadsen, and Louise Barny Christensen, Hvidovre Hospital, for technical support. We thank Carles Martínez and Adolfo Garcia-Sastre (Icahn School of Medicine, Mount Sinai) for providing Calu-3 cells and Charles Rice (Rockefeller University) for providing Huh7.5 cells.

This study was supported by grants from the Region H Foundation (S.R., J.M.G., J.B.), the Novo Nordisk Foundation (J.B.), Independent Research Fund Denmark (DFF), Medical Sciences (S.R., J.M.G., J.B.), the Candys Foundation (C.F.-A., L.V.P., J.B.), the Weimann Foundation (U.F.), the Læge Sophus Carl Emil Friis og hustru Olga Doris Friis Legat (J.M.G.), and the Danish Agency for Science and Higher Education (S.R., J.B.). J.B. is the 2015 recipient of the Novo Nordisk Prize and the 2019 recipient of a Distinguished Investigator grant from the Novo Nordisk Foundation.

REFERENCES

1. Lu R, Zhao X, Li J, Niu P, Yang B, Wu H, Wang W, Song H, Huang B, Zhu N, Bi Y, Ma X, Zhan F, Wang L, Hu T, Zhou H, Hu Z, Zhou W, Zhao L, Chen J, Meng Y, Wang J, Lin Y, Yuan J, Xie Z, Ma J, Liu WJ, Wang D, Xu W, Holmes EC, Gao GF, Wu G, Chen W, Shi W, Tan W. 2020. Genomic characterisation and epidemiology of 2019 novel coronavirus: implications for virus origins and receptor binding. Lancet 395:565–574. https://doi.org/10.1016/S0140-6736(20)30251-8.
2. Dong E, Du H, Gardner L. 2020. An interactive Web-based dashboard to track COVID-19 in real time. Lancet Infect Dis 20:533–534. https://doi.org/10.1016/S1473-3099(20)30120-1.
3. Ackermann M, Verleden SE, Kuehnel M, Haverich A, Welte T, Laenger F, Vanstapel A, Werlein C, Stark H, Tzankov A, Li WW, Li VW, Mentzer SJ, Jonigk D. 2020. Pulmonary vascular endothelialitis, thrombosis, and angiogenesis in Covid-19. N Engl J Med 383:120–128. https://doi.org/10.1056/NEJMoa2015432.
4. Gupta A, Madhavan MV, Sehgal K, Nair N, Mahajan S, Sehrawat TS, Bikdeli B, Ahluwalia N, Ausiello JC, Wan EY, Freedberg DE, Kirtane AJ, Parikh SA, Maurer MS, Nordvig AS, Accili D, Bathon JM, Mohan S, Bauer KA, Leon MB, Krumholz HM, Uriel N, Mehra MR, Elkind MSV, Stone GW, Schwartz A, Ho DD, Bilezikian JP, Landry DW. 2020. Extrapulmonary manifestations of COVID-19. Nat Med 26:1017–1032. https://doi.org/10.1038/s41591-020-0968-3.
5. Puelles VG, Lütgehetmann M, Lindenmeyer MT, Sperhake JP, Wong MN, Allweiss L, Chilla S, Heinemann A, Wanner N, Liu S, Braun F, Lu S, Pfefferle S, Schröder AS, Edler C, Gross O, Glatzel M, Wichmann D, Wiech T, Kluge S, Pueschel K, Aepfelbacher M, Huber TB. 2020. Multiorgan and renal tropism of SARS-CoV-2. N Engl J Med 383:590–592. https://doi.org/10.1056/NEJMc2011400.
6. Coronaviridae Study Group of the International Committee on Taxonomy of Viruses. 2020. The species severe acute respiratory syndrome-related coronavirus: classifying 2019-nCoV and naming it SARS-CoV-2. Nat Microbiol 5:536–544. https://doi.org/10.1038/s41564-020-0695-z.
7. Pruijssers AJ, Denison MR. 2019. Nucleoside analogues for the treatment of coronavirus infections. Curr Opin Virol 35:57–62. https://doi.org/10.1016/j.coviro.2019.04.002.
8. Stuyver LJ, Whitaker T, McBrayer TR, Hernandez-Santiago BI, Lostia S, Tharnish PM, Ramesh M, Chu CK, Jordan R, Shi J, Rachakonda S, Watanabe KA, Otto MJ, Schinazi RF. 2003. Ribonucleoside analogue that blocks replication of bovine viral diarrhea and hepatitis C viruses in culture.

Antimicrob Agents Chemother 47:244–254. https://doi.org/10.1128/aac.47.1.244-254.2003.
9. Cho A, Saunders OL, Butler T, Zhang L, Xu J, Vela JE, Feng JY, Ray AS, Kim CU. 2012. Synthesis and antiviral activity of a series of 1′-substituted 4-aza-7,9-dideazaadenosine C-nucleosides. Bioorg Med Chem Lett 22:2705–2707. https://doi.org/10.1016/j.bmcl.2012.02.105.
10. Takayama K. 2020. In vitro and animal models for SARS-CoV-2 research. Trends Pharmacol Sci 41:513–517. https://doi.org/10.1016/j.tips.2020.05.005.
11. Pruijssers AJ, George AS, Schäfer A, Leist SR, Gralinksi LE, Dinnon KH, III, Yount BL, Agostini ML, Stevens LJ, Chappell JD, Lu X, Hughes TM, Gully K, Martinez DR, Brown AJ, Graham RL, Perry JK, Du Pont V, Pitts J, Ma B, Babusis D, Murakami E, Feng JY, Bilello JP, Porter DP, Cihlar T, Baric RS, Denison MR, Sheahan TP. 2020. Remdesivir inhibits SARS-CoV-2 in human lung cells and chimeric SARS-CoV expressing the SARS-CoV-2 RNA polymerase in mice. Cell Rep 32:107940. https://doi.org/10.1016/j.celrep.2020.107940.
12. Blanco R, Iwakawa R, Tang M, Kohno T, Angulo B, Pio R, Montuenga LM, Minna JD, Yokota J, Sanchez-Cespedes M. 2009. A gene-alteration profile of human lung cancer cell lines. Hum Mutat 30:1199–1206. https://doi.org/10.1002/humu.21028.
13. Matsuyama S, Nao N, Shirato K, Kawase M, Saito S, Takayama I, Nagata N, Sekizuka T, Katoh H, Kato F, Sakata M, Tahara M, Kutsuna S, Ohmagari N, Kuroda M, Suzuki T, Kageyama T, Takeda M. 2020. Enhanced isolation of SARS-CoV-2 by TMPRSS2-expressing cells. Proc Natl Acad Sci U S A 117:7001–7003. https://doi.org/10.1073/pnas.2002589117.
14. Xie X, Muruato AE, Zhang X, Lokugamage KG, Fontes-Garfias CR, Zou J, Liu J, Ren P, Balakrishnan M, Cihlar T, Tseng C-TK, Makino S, Menachery VD, Bilello JP, Shi P-Y. 2020. A nanoluciferase SARS-CoV-2 for rapid neutralization testing and screening of anti-infective drugs for COVID-19. Nat Commun 11:5214. https://doi.org/10.1038/s41467-020-19055-7.
15. Weston S, Coleman CM, Haupt R, Logue J, Matthews K, Li Y, Reyes HM, Weiss SR, Frieman MB. 2020. Broad anti-coronavirus activity of Food and Drug Administration-approved drugs against SARS-CoV-2 in vitro and SARS-CoV in vivo. J Virol 94:e01218-20. https://doi.org/10.1128/JVI.01218-20.
16. Stanifer ML, Kee C, Cortese M, Zumaran CM, Triana S, Mukenhirn M, Kraeusslich H-G, Alexandrov T, Bartenschlager R, Boulant S. 2020. Critical role of type III interferon in controlling SARS-CoV-2 infection in human intestinal epithelial cells. Cell Rep 32:107863. https://doi.org/10.1016/j.celrep.2020.107863.
17. Blight KJ, McKeating JA, Rice CM. 2002. Highly permissive cell lines for subgenomic and genomic hepatitis C virus RNA replication. J Virol 76:13001–13014. https://doi.org/10.1128/jvi.76.24.13001-13014.2002.
18. Ramirez S, Bukh J. 2018. Current status and future development of infectious cell-culture models for the major genotypes of hepatitis C virus: essential tools in testing of antivirals and emerging vaccine strategies. Antiviral Res 158:264–287. https://doi.org/10.1016/j.antiviral.2018.07.014.
19. Korber B, Fischer WM, Gnanakaran S, Yoon H, Theiler J, Abfalterer W, Hengartner N, Giorgi EE, Bhattacharya T, Foley B, Hastie KM, Parker MD, Partridge DG, Evans CM, Freeman TM, de Silva TI, Sheffield COVID-19 Genomics Group, McDanal C, Perez LG, Tang H, Moon-Walker A, Whelan SP, LaBranche CC, Saphire EO, Montefiori DC. 2020. Tracking changes in SARS-CoV-2 spike: evidence that D614G increases infectivity of the COVID-19 virus. Cell 182:812–827.e19. https://doi.org/10.1016/j.cell.2020.06.043.
20. Hou YJ, Chiba S, Halfmann P, Ehre C, Kuroda M, Dinnon KH, III, Leist SR, Schäfer A, Nakajima N, Takahashi K, Lee RE, Mascenik TM, Graham R, Edwards CE, Tse LV, Okuda K, Markmann AJ, Bartelt L, de Silva A, Margolis DM, Boucher RC, Randell SH, Suzuki T, Gralinski LE, Kawaoka Y, Baric RS. 2020. SARS-CoV-2 D614G variant exhibits efficient replication ex vivo and transmission in vivo. Science 370:1464–1468. https://doi.org/10.1126/science.abe8499.
21. Wei C, Wan L, Yan Q, Wang X, Zhang J, Yang X, Zhang Y, Fan C, Li D, Deng Y, Sun J, Gong J, Yang X, Wang Y, Wang X, Li J, Yang H, Li H, Zhang Z, Wang R, Du P, Zong Y, Yin F, Zhang W, Wang N, Peng Y, Lin H, Feng J, Qin C, Chen W, Gao Q, Zhang R, Cao Y, Zhong H. 2020. HDL-scavenger receptor B type 1 facilitates SARS-CoV-2 entry. Nat Metab 2:1391–1400. https://doi.org/10.1038/s42255-020-00324-0.
22. Zhu H, Wong-Staal F, Lee H, Syder A, McKelvy J, Schooley RT, Wyles DL. 2012. Evaluation of ITX 5061, a scavenger receptor B1 antagonist: resistance selection and activity in combination with other hepatitis C virus antivirals. J Infect Dis 205:656–662. https://doi.org/10.1093/infdis/jir802.
23. Pizzorno A, Padey B, Dubois J, Julien T, Traversier A, Dulière V, Brun P, Lina B, Rosa-Calatrava M, Terrier O. 2020. In vitro evaluation of antiviral activity of single and combined repurposable drugs against SARS-CoV-2. Antiviral Res 181:104878. https://doi.org/10.1016/j.antiviral.2020.104878.
24. Choy K-T, Wong AY-L, Kaewpreedee P, Sia SF, Chen D, Hui KPY, Chu DKW, Chan MCW, Cheung PP-H, Huang X, Peiris M, Yen H-L. 2020. Remdesivir, lopinavir, emetine, and homoharringtonine inhibit SARS-CoV-2 replication in vitro. Antiviral Res 178:104786. https://doi.org/10.1016/j.antiviral.2020.104786.
25. Ogando NS, Dalebout TJ, Zevenhoven-Dobbe JC, Limpens RWAL, van der Meer Y, Caly L, Druce J, de Vries JJC, Kikkert M, Bárcena M, Sidorov I, Snijder EJ. 2020. SARS-coronavirus-2 replication in Vero E6 cells: replication kinetics, rapid adaptation and cytopathology. J Gen Virol 101:925–940. https://doi.org/10.1099/jgv.0.001453.
26. Sofia MJ. 2016. Enter sofosbuvir: the path to curing HCV. Cell 167:25–29. https://doi.org/10.1016/j.cell.2016.08.044.
27. Sheahan TP, Sims AC, Zhou S, Graham RL, Pruijssers AJ, Agostini ML, Leist SR, Schäfer A, Dinnon KH, III, Stevens LJ, Chappell JD, Lu X, Hughes TM, George AS, Hill CS, Montgomery SA, Brown AJ, Bluemling GR, Natchus MG, Saindane M, Kolykhalov AA, Painter G, Harcourt J, Tamin A, Thornburg NJ, Swanstrom R, Denison MR, Baric RS. 2020. An orally bioavailable broad-spectrum antiviral inhibits SARS-CoV-2 in human airway epithelial cell cultures and multiple coronaviruses in mice. Sci Transl Med 12:eabb5883. https://doi.org/10.1126/scitranslmed.abb5883.
28. Cavazzoni A, Galetti M, Fumarola C, Alfieri RR, Roz L, Andriani F, Carbognani P, Rusca M, Sozzi G, Petronini PG. 2007. Effect of inducible FHIT and p53 expression in the Calu-1 lung cancer cell line. Cancer Lett 246:69–81. https://doi.org/10.1016/j.canlet.2006.01.033.
29. Gazdar AF, Girard L, Lockwood WW, Lam WL, Minna JD. 2010. Lung cancer cell lines as tools for biomedical discovery and research. J Natl Cancer Inst 102:1310–1321. https://doi.org/10.1093/jnci/djq279.
30. van Diepen A, Brand HK, Sama I, Lambooy LHJ, van den Heuvel LP, van der Well L, Huynen M, Osterhaus ADME, Andeweg AC, Hermans PWM. 2010. Quantitative proteome profiling of respiratory virus-infected lung epithelial cells. J Proteomics 73:1680–1693. https://doi.org/10.1016/j.jprot.2010.04.008.
31. Han J, Perez JT, Chen C, Li Y, Benitez A, Kandasamy M, Lee Y, Andrade J, tenOever B, Manicassamy B. 2018. Genome-wide CRISPR/Cas9 screen identifies host factors essential for influenza virus replication. Cell Rep 23:596–607. https://doi.org/10.1016/j.celrep.2018.03.045.
32. Sumpter R, Wang C, Foy E, Loo Y-M, Gale M. 2004. Viral evolution and interferon resistance of hepatitis C virus RNA replication in a cell culture model. J Virol 78:11591–11604. https://doi.org/10.1128/JVI.78.21.11591-11604.2004.
33. Tang BSF, Chan K-H, Cheng VCC, Woo PCY, Lau SKP, Lam CCK, Chan T-L, Wu AKL, Hung IFN, Leung S-Y, Yuen K-Y. 2005. Comparative host gene transcription by microarray analysis early after infection of the Huh7 cell line by severe acute respiratory syndrome coronavirus and human coronavirus 229E. J Virol 79:6180–6193. https://doi.org/10.1128/JVI.79.10.6180-6193.2005.
34. Felgenhauer U, Schoen A, Gad HH, Hartmann R, Schaubmar AR, Failing K, Drosten C, Weber F. 2020. Inhibition of SARS-CoV-2 by type I and type III interferons. J Biol Chem 295:13958–13964. https://doi.org/10.1074/jbc.AC120.013788.
35. Emeny JM, Morgan MJ. 1979. Regulation of the interferon system: evidence that Vero cells have a genetic defect in interferon production. J Gen Virol 43:247–252. https://doi.org/10.1099/0022-1317-43-1-247.
36. van Dorp L, Richard D, Tan CCS, Shaw LP, Acman M, Balloux F. 2020. No evidence for increased transmissibility from recurrent mutations in SARS-CoV-2. Nat Commun 11:5986. https://doi.org/10.1038/s41467-020-19818-2.
37. Shajahan A, Supekar NT, Gleinich AS, Azadi P. 2020. Deducing the N- and O-glycosylation profile of the spike protein of novel coronavirus SARS-CoV-2. Glycobiology 30:981–988. https://doi.org/10.1093/glycob/cwaa042.
38. Leung K, Shum MHH, Leung GM, Lam TTY, Wu JT. 2021. Early transmissibility assessment of the N501Y mutant strains of SARS-CoV-2 in the United Kingdom, October to November 2020. Euro Surveill 26:2002106. https://doi.org/10.2807/1560-7917.ES.2020.26.1.2002106.
39. Wang Q, Zhang Y, Wu L, Niu S, Song C, Zhang Z, Lu G, Qiao C, Hu Y, Yuen K-Y, Wang Q, Zhou H, Yan J, Qi J. 2020. Structural and functional basis of SARS-CoV-2 entry by using human ACE2. Cell 181:894–904.e9. https://doi.org/10.1016/j.cell.2020.03.045.
40. Chen J, Wang R, Wang M, Wei G-W. 2020. Mutations strengthened SARS-CoV-2 infectivity. J Mol Biol 432:5212–5226. https://doi.org/10.1016/j.jmb.2020.07.009.
41. Hoffmann M, Kleine-Weber H, Schroeder S, Krüger N, Herrler T, Erichsen S, Schiergens TS, Herrler G, Wu N-H, Nitsche A, Müller MA, Drosten C, Pöhlmann S. 2020. SARS-CoV-2 cell entry depends on ACE2 and TMPRSS2 and is blocked by a clinically proven protease inhibitor. Cell 181:271–280.e8. https://doi.org/10.1016/j.cell.2020.02.052.

42. Hoffmann M, Kleine-Weber H, Pöhlmann S. 2020. A multibasic cleavage site in the spike protein of SARS-CoV-2 is essential for infection of human lung cells. Mol Cell 78:779–784.e5. https://doi.org/10.1016/j.molcel.2020.04.022.
43. Belouzard S, Chu VC, Whittaker GR. 2009. Activation of the SARS coronavirus spike protein via sequential proteolytic cleavage at two distinct sites. Proc Natl Acad Sci U S A 106:5871–5876. https://doi.org/10.1073/pnas.0809524106.
44. Watanabe R, Matsuyama S, Shirato K, Maejima M, Fukushi S, Morikawa S, Taguchi F. 2008. Entry from the cell surface of severe acute respiratory syndrome coronavirus with cleaved S protein as revealed by pseudotype virus bearing cleaved S protein. J Virol 82:11985–11991. https://doi.org/10.1128/JVI.01412-08.
45. Yamada Y, Liu DX. 2009. Proteolytic activation of the spike protein at a novel RRRR/S motif is implicated in furin-dependent entry, syncytium formation, and infectivity of coronavirus infectious bronchitis virus in cultured cells. J Virol 83:8744–8758. https://doi.org/10.1128/JVI.00613-09.
46. Klimstra WB, Tilston-Lunel NL, Nambulli S, Boslett J, McMillen CM, Gilliland T, Dunn MD, Sun C, Wheeler SE, Wells A, Hartman AL, McElroy AK, Reed DS, Rennick LJ, Duprex WP. 2020. SARS-CoV-2 growth, furin-cleavage-site adaptation and neutralization using serum from acutely infected hospitalized COVID-19 patients. J Gen Virol 101:1156–1169. https://doi.org/10.1099/jgv.0.001481.
47. Xia S, Liu M, Wang C, Xu W, Lan Q, Feng S, Qi F, Bao L, Du L, Liu S, Qin C, Sun F, Shi Z, Zhu Y, Jiang S, Lu L. 2020. Inhibition of SARS-CoV-2 (previously 2019-nCoV) infection by a highly potent pan-coronavirus fusion inhibitor targeting its spike protein that harbors a high capacity to mediate membrane fusion. Cell Res 30:343–355. https://doi.org/10.1038/s41422-020-0305-x.
48. Chu H, Chan JF-W, Yuen TT-T, Shuai H, Yuan S, Wang Y, Hu B, Yip CC-Y, Tsang JO-L, Huang X, Chai Y, Yang D, Hou Y, Chik KK-H, Zhang X, Fung AY-F, Tsoi H-W, Cai J-P, Chan W-M, Ip JD, Chu AW-H, Zhou J, Lung DC, Kok K-H, To KK-W, Tsang OT-Y, Chan K-H, Yuen K-Y. 2020. Comparative tropism, replication kinetics, and cell damage profiling of SARS-CoV-2 and SARS-CoV with implications for clinical manifestations, transmissibility, and laboratory studies of COVID-19: an observational study. Lancet Microbe 1:e14–e23. https://doi.org/10.1016/S2666-5247(20)30004-5.
49. Nie Y, Wang P, Shi X, Wang G, Chen J, Zheng A, Wang W, Wang Z, Qu X, Luo M, Tan L, Song X, Yin X, Chen J, Ding M, Deng H. 2004. Highly infectious SARS-CoV pseudotyped virus reveals the cell tropism and its correlation with receptor expression. Biochem Biophys Res Commun 321:994–1000. https://doi.org/10.1016/j.bbrc.2004.07.060.
50. Hamming I, Timens W, Bulthuis MLC, Lely AT, Navis GJ, van Goor H. 2004. Tissue distribution of ACE2 protein, the functional receptor for SARS coronavirus. A first step in understanding SARS pathogenesis. J Pathol 203:631–637. https://doi.org/10.1002/path.1570.
51. Ma D, Chen C-B, Jhanji V, Xu C, Yuan X-L, Liang J-J, Huang Y, Cen L-P, Ng TK. 2020. Expression of SARS-CoV-2 receptor ACE2 and TMPRSS2 in human primary conjunctival and pterygium cell lines and in mouse cornea. Eye (Lond) 34:1212–1219. https://doi.org/10.1038/s41433-020-0939-4.
52. Cantuti-Castelvetri L, Ojha R, Pedro LD, Djannatian M, Franz J, Kuivanen S, van der Meer F, Kallio K, Kaya T, Anastasina M, Smura T, Levanov L, Szirovicza L, Tobi A, Kallio-Kokko H, Österlund P, Joensuu M, Meunier FA, Butcher SJ, Winkler MS, Mollenhauer B, Helenius A, Gokce O, Teesalu T, Hepojoki J, Vapalahti O, Stadelmann C, Balistreri G, Simons M. 2020. Neuropilin-1 facilitates SARS-CoV-2 cell entry and infectivity. Science 370:856–860. https://doi.org/10.1126/science.abd2985.
53. Clausen TM, Sandoval DR, Spliid CB, Pihl J, Perrett HR, Painter CD, Narayanan A, Majowicz SA, Kwong EM, McVicar RN, Thacker BE, Glass CA, Yang Z, Torres JL, Golden GJ, Bartels PL, Porell RN, Garretson AF, Laubach L, Feldman J, Yin X, Pu Y, Hauser BM, Caradonna TM, Kellman BP, Martino C, Gordts PLSM, Chanda SK, Schmidt AG, Godula K, Leibel SL, Jose J, Corbett KD, Ward AB, Carlin AF, Esko JD. 2020. SARS-CoV-2 infection depends on cellular heparan sulfate and ACE2. Cell 183:1043–1057.e15. https://doi.org/10.1016/j.cell.2020.09.033.
54. Zmora P, Moldenhauer A-S, Hofmann-Winkler H, Pöhlmann S. 2015. TMPRSS2 isoform 1 activates respiratory viruses and is expressed in viral target cells. PLoS One 10:e0138380. https://doi.org/10.1371/journal.pone.0138380.
55. Esumi M, Ishibashi M, Yamaguchi H, Nakajima S, Tai Y, Kikuta S, Sugitani M, Takayama T, Tahara M, Takeda M, Wakita T. 2015. Transmembrane serine protease TMPRSS2 activates hepatitis C virus infection. Hepatology 61:437–446. https://doi.org/10.1002/hep.27426.
56. Yan VC, Muller FL. 2020. Advantages of the parent nucleoside GS-441524 over remdesivir for Covid-19 treatment. ACS Med Chem Lett 11:1361–1366. https://doi.org/10.1021/acsmedchemlett.0c00316.
57. Li YP, Ramirez S, Jensen SB, Purcell RH, Gottwein JM, Bukh J. 2012. Highly efficient full-length hepatitis C virus genotype 1 (strain TN) infectious culture system. Proc Natl Acad Sci U S A 109:19757–19762. https://doi.org/10.1073/pnas.1218260109.
58. Ramirez S, Mikkelsen LS, Gottwein JM, Bukh J. 2016. Robust HCV genotype 3a infectious cell culture system permits identification of escape variants with resistance to sofosbuvir. Gastroenterology 151:973–985.e2. https://doi.org/10.1053/j.gastro.2016.07.013.
59. Ramirez S, Li YP, Jensen SB, Pedersen J, Gottwein JM, Bukh J. 2014. Highly efficient infectious cell culture of three hepatitis C virus genotype 2b strains and sensitivity to lead protease, nonstructural protein 5A, and polymerase inhibitors. Hepatology 59:395–407. https://doi.org/10.1002/hep.26660.
60. Ramirez S, Fernandez-Antunez C, Mikkelsen LS, Pedersen J, Li Y-P, Bukh J. 2020. Cell culture studies of the efficacy and barrier to resistance of sofosbuvir-velpatasvir and glecaprevir-pibrentasvir against hepatitis C virus genotypes 2a, 2b, and 2c. Antimicrob Agents Chemother 64:e01888-19. https://doi.org/10.1128/AAC.01888-19.
61. Toots M, Yoon J-J, Cox RM, Hart M, Sticher ZM, Makhsous N, Plesker R, Barrena AH, Reddy PG, Mitchell DG, Shean RC, Bluemling GR, Kolykhalov AA, Greninger AL, Natchus MG, Painter GR, Plemper RK. 2019. Characterization of orally efficacious influenza drug with high resistance barrier in ferrets and human airway epithelia. Sci Transl Med 11:eaax5866. https://doi.org/10.1126/scitranslmed.aax5866.
62. Jácome R, Campillo-Balderas JA, Ponce de León S, Becerra A, Lazcano A. 2020. Sofosbuvir as a potential alternative to treat the SARS-CoV-2 epidemic. Sci Rep 10:9294. https://doi.org/10.1038/s41598-020-66440-9.
63. Chien M, Anderson TK, Jockusch S, Tao C, Li X, Kumar S, Russo JJ, Kirchdoerfer RN, Ju J. 2020. Nucleotide analogues as inhibitors of SARS-CoV-2 polymerase, a key drug target for COVID-19. J Proteome Res 19:4690–4697. https://doi.org/10.1021/acs.jproteome.0c00392.
64. Shannon A, Le NT-T, Selisko B, Eydoux C, Alvarez K, Guillemot J-C, Decroly E, Peersen O, Ferron F, Canard B. 2020. Remdesivir and SARS-CoV-2: structural requirements at both nsp12 RdRp and nsp14 exonuclease active-sites. Antiviral Res 178:104793. https://doi.org/10.1016/j.antiviral.2020.104793.
65. Takahashi H, Iwasaki Y, Watanabe T, Ichinose N, Okada Y, Oiwa A, Kobayashi T, Moriya M, Oda T. 2020. Case studies of SARS-CoV-2 treated with favipiravir among patients in critical or severe condition. Int J Infect Dis 100:283–285. https://doi.org/10.1016/j.ijid.2020.08.047.
66. Bekerman E, Einav S. 2015. Infectious disease. Combating emerging viral threats. Science 348:282–283. https://doi.org/10.1126/science.aaa3778.
67. Wang P, Nair MS, Liu L, Iketani S, Luo Y, Guo Y, Wang M, Yu J, Zhang B, Kwong PD, Graham BS, Mascola JR, Chang JY, Yin MT, Sobieszczyk M, Kyratsous CA, Shapiro L, Sheng Z, Huang Y, Ho DD. 8 March 2021. Antibody resistance of SARS-CoV-2 variants B.1.351 and B.1.1.7. Nature https://doi.org/10.1038/s41586-021-03398-2.
68. Corman VM, Landt O, Kaiser M, Molenkamp R, Meijer A, Chu DKW, Bleicker T, Brünink S, Schneider J, Schmidt ML, Mulders DGJC, Haagmans BL, van der Veer B, van den Brink S, Wijsman L, Goderski G, Romette J-L, Ellis J, Zambon M, Peiris M, Goossens H, Reusken C, Koopmans MPG, Drosten C. 2020. Detection of 2019 novel coronavirus (2019-nCoV) by real-time RT-PCR. Euro Surveill 25:2000045. https://doi.org/10.2807/1560-7917.ES.2020.25.3.2000045.
69. Lindenbach BD, Evans MJ, Syder AJ, Wolk B, Tellinghuisen TL, Liu CC, Maruyama T, Hynes RO, Burton DR, McKeating JA, Rice CM. 2005. Complete replication of hepatitis C virus in cell culture. Science 309:623–626. https://doi.org/10.1126/science.1114016.
70. Knipe DM, Howley PM, Griffin DE, Lamb RA, Martin MA, Roizman B, Straus SE (ed). 2007. Fields virology, 5th ed. Lippincott Williams & Wilkins, Philadelphia, PA.
71. Fahnoe U, Bukh J. 2019. Full-length open reading frame amplification of hepatitis C virus. Methods Mol Biol 1911:85–91. https://doi.org/10.1007/978-1-4939-8976-8_5.
72. Li YP, Gottwein JM, Scheel TK, Jensen TB, Bukh J. 2011. MicroRNA-122 antagonism against hepatitis C virus genotypes 1-6 and reduced efficacy by host RNA insertion or mutations in the HCV 5′ UTR. Proc Natl Acad Sci U S A 108:4991–4996. https://doi.org/10.1073/pnas.1016606108.
73. Jensen SB, Fahnoe U, Pham LV, Serre S, Tang Q, Ghanem L, Pedersen MS, Ramirez S, Humes D, Pihl AF, Filskov J, Solund CS, Dietz J, Fourati S, Pawlotsky JM, Sarrazin C, Weis N, Schonning K, Krarup H, Bukh J, Gottwein JM. 2019. Evolutionary pathways to persistence of highly fit and resistant hepatitis C virus protease inhibitor escape variants. Hepatology 70:771–787. https://doi.org/10.1002/hep.30647.
74. Martin M. 2011. Cutadapt removes adapter sequences from high-throughput sequencing reads. EMBnet J 17:10–12. https://doi.org/10.14806/ej.17.1.200.
75. Gottwein JM, Scheel TKH, Callendret B, Li Y-P, Eccleston HB, Engle RE, Govindarajan S, Satterfield W, Purcell RH, Walker CM, Bukh J. 2010. Novel

infectious cDNA clones of hepatitis C virus genotype 3a (strain S52) and 4a (strain ED43): genetic analyses and in vivo pathogenesis studies. J Virol 84:5277–5293. https://doi.org/10.1128/JVI.02667-09.
76. Gottwein JM, Scheel TK, Jensen TB, Ghanem L, Bukh J. 2011. Differential efficacy of protease inhibitors against HCV genotypes 2a, 3a, 5a, and 6a NS3/4A protease recombinant viruses. Gastroenterology 141:1067–1079. https://doi.org/10.1053/j.gastro.2011.06.004.
77. Iglewicz B, Hoaglin DC. 1993. How to detect and handle outliers. ASQC Quality Press, Milwaukee, WI.
78. Edgar RC. 2004. MUSCLE: multiple sequence alignment with high accuracy and high throughput. Nucleic Acids Res 32:1792–1797. https://doi.org/10.1093/nar/gkh340.
79. Yuan Y, Cao D, Zhang Y, Ma J, Qi J, Wang Q, Lu G, Wu Y, Yan J, Shi Y, Zhang X, Gao GF. 2017. Cryo-EM structures of MERS-CoV and SARS-CoV spike glycoproteins reveal the dynamic receptor binding domains. Nat Commun 8:15092. https://doi.org/10.1038/ncomms15092.
80. Park Y-J, Walls AC, Wang Z, Sauer MM, Li W, Tortorici MA, Bosch B-J, DiMaio F, Veesler D. 2019. Structures of MERS-CoV spike glycoprotein in complex with sialoside attachment receptors. Nat Struct Mol Biol 26:1151–1157. https://doi.org/10.1038/s41594-019-0334-7.
81. Bangaru S, Ozorowski G, Turner HL, Antanasijevic A, Huang D, Wang X, Torres JL, Diedrich JK, Tian J-H, Portnoff AD, Patel N, Massare MJ, Yates JR, Nemazee D, Paulson JC, Glenn G, Smith G, Ward AB. 2020. Structural analysis of full-length SARS-CoV-2 spike protein from an advanced vaccine candidate. Science 370:1089–1094. https://doi.org/10.1126/science.abe1502.
82. Schrödinger LLC. 2019. The PyMOL molecular graphics system, version 2.3. Schrödinger LLC, New York, NY.
83. Fiser A, Sali A. 2003. ModLoop: automated modeling of loops in protein structures. Bioinformatics 19:2500–2501. https://doi.org/10.1093/bioinformatics/btg362.
84. Gui M, Song W, Zhou H, Xu J, Chen S, Xiang Y, Wang X. 2017. Cryo-electron microscopy structures of the SARS-CoV spike glycoprotein reveal a prerequisite conformational state for receptor binding. Cell Res 27:119–129. https://doi.org/10.1038/cr.2016.152.